Contents lists available at ScienceDirect

Solar Energy

journal homepage: http://ees.elsevier.com

Thermal performance analysis of a new structured-core translucent vacuum insulation panel in comparison to vacuum glazing: Experimental and theoretically validated analyses

Takao Katsura [a,*], Saim Memon [b], Ali Radwan [a,c], Makoto Nakamura [a], Katsunori Nagano [a]

[a] Division of Human Environmental Systems, Faculty of Engineering, Hokkaido University, N13-W8, Kita-ku, Sapporo 060-8628, Japan
[b] London Centre for Energy Engineering, Division of Electrical and Electronic Engineering, School of Engineering, London South Bank University, 103 Borough Road, London SE1 0AA, UK
[c] Mechanical Power Engineering Department, Faculty of Engineering, Mansoura University, Mansoura 35516, Egypt

ARTICLE INFO

Keywords
Vacuum glazing
Translucent vacuum insulation panel
Thermal performance
Energy conservation
Finite-volume modelling
Nearly zero energy buildings

ABSTRACT

The notion at which, nowadays, building sector is being recognized to be nearly zero-energy buildings (NZEBs) relies partly on the thermal performance of its fabric insulation. Vacuum glazing (VG) technology attracted the research interest as an option to reduce heat loss through windows. However, the total glazing thermal transmittance (U-value) for VG increases with the use of smaller glazing size due to the edge-seal effects, due to the thermal short-circuit around the edges, and the overall construction cost of it leading to an unaffordable option to deal with energy conservation of buildings. Therefore, this study aims to propose a new structured core transparent vacuum insulation panel (TVIP) to accomplish insulation for the windows without edge sealing effect, with lower cost, and can be easily retrofitted to the conventional windows of the existing buildings. To do this, VG and TVIP were constructed and their thermal conductivity were measured using heat flow meter apparatus. In addition, a 3D finite volume model considering the effect of vacuum surface to surface radiation, gas conduction, and thermal bridges through the spacer material and sealing material is developed. The model is validated with the experiments and with the data for VG in the literature. The effect of an increase of vacuum pressure is simulated and the vacuum deterioration problem and the glazing size on the insulation performance of both VG and TVIP were investigated. The results indicate that for a smaller glazing area of less than 30 cm × 30 cm, the TVIP accomplished lower U-value compared with the VG at vacuum pressure of 0.1 Pa and 1 Pa. While, at a vacuum pressure of 10 Pa, the TVIP attained a lower U-value over the entire range of glazing sizes. Further, the edge-seal effect in the VG is diminished with the use of TVIP. Furthermore, the material cost per unit area of the TVIP is three times less than the cost of VG at laboratory scale. The results of the current study can guide vacuum window designers and researchers to further enhance the performance of TVIP based window to compete for the VG in the markets.

Nomenclature

k	thermal conductivity [$Wm^{-1}K^{-1}$]
l_v	VIP thickness [m]
P	pressure [Nm^{-2}]
q	heat flux either on the hot or the cold side of the VIP [Wm^{-2}]
T	temperature [^{o} C]
h	convection heat transfer coefficient from either the cold or hot side of the glazing's [$Wm^{-2}K^{-1}$]
S	source term in the energy equation [Wm^{-3}]
U	thermal transmittance [$Wm^{-2}K^{-1}$]

Greek symbols

Δ	difference
δ	thickness [m]
k_o	air thermal conductivity [$Wm^{-1}K^{-1}$]
k_v	vacuum space thermal conductivity [$Wm^{-1}K^{-1}$]

Subscripts

c	cold side of the VIP
g	glass
∞	free stream
v	VIP

Abbreviations

Corresponding author
Corresponding author
E-mail addresses: katsura@eng.hokudai.ac.jp (T. Katsura); S.Memon@lsbu.ac.uk (S. Memon)

https://doi.org/10.1016/j.solener.2020.02.030
Received 10 November 2019; Received in revised form 23 January 2020; Accepted 7 Febraury 2020
Available online xxx
0038-092/

CPP	cast polypropylene
FEM	finite element model
FVM	finite volume model
HFM	heat flow meter.
HSS	heat seal strength
MTP	moisture transmission rate
OTR	oxygen transmission rate
PA	polymide
PET	polyethylene terapthalate
PLC	programmable logic controller
SE	silica evaporated
TVIP	translucent vacuum insulation panel
VG	vacuum glazing
VIP	vacuum insulation panel

1. Introduction

The notion at which, nowadays, building sector is being recognized to be nearly zero energy buildings (NZEBs) relies partly on the thermal performance of its fabric insulation (Brambilla et al., 2018). Correspondingly, glazed windows play an imperative part in terms of allowing natural daylighting (Memon and Eames, 2017) with the consequences of the space-heating loss in hot-arid and space-cooling loss in cold-arid climates. The advancements and integration of progressive vacuum insulation technologies are one of the realistic solutions in making the domestic and commercial buildings to NZEBs and/or zero energy buildings (ZEB). This because, the energy consumption in buildings is increasing very fast. In addition, the consumption of energy in buildings has exceeded the industrial and traffic energy consumption in the developed countries (Zhu et al., 2020). In more details, around 40% of the global primary energy is consumed by buildings and contribute to around 30% of carbon dioxide emissions (Pérez-Lombard et al., 2008). Among building services, the energy consumption by HVAC systems is particularly significant which represent around 50% of the building energy consumption and around 20% of the total energy consumption in some developed countries (Pérez-Lombard et al., 2008). Normally, the high energy consumption by HVAC system is a linked with poor thermal insulation for the building structure including walls, and transparent facades. However, the normal structure of the building exterior walls has a thermal transmission coefficient (U-value) ranging from 0.047 to 0.11 $Wm^{-2}K^{-1}$, while the standard U-value was 0.282 $Wm^{-2}K^{-1}$ (Kisilewicz et al., 2019). The lower U-value for exterior walls can be accomplished using opaque vacuum insulated panels (VIP) through the wall structure (Johansson et al., 2014). On the other hand, transparent facades including windows are suffering from high U-value of 5.7 $Wm^{-2}K^{-1}$ for 6 mm thick glazing's (Huang et al., 2020). Further, developing buildings with large glazing's exterior facades nowadays makes the high thermal insulation for windows a crucial issue. Therefore, thermal insulation methods for windows including vacuum glazing (VG), double glazing with air gap, triple vacuum glazing, and air-vacuum layered triple glazed windows are gaining popularity nowadays (Fang et al., 2020).

Glazing facades and windows visually connect the building interiors to the outdoor environment to promote resident relaxation and keep a comfortable daylight (Ghosh and Norton, 2018). One of these glazing's is vacuum glazing's VG. The VG consists of two panes of glass separated by an evacuated gap at very low pressure less than 0.1 Pa. These two glass panes were supported with a very tiny pillars normally made of stainless steel and hermetically sealed (Memon et al., 2019). These VG proved its low U-value between 1.1 $Wm^{-2}K^{-1}$ and 0.8 $Wm^{-2}K^{-1}$ at a pressure of 0.1 Pa (Fang et al., 2014). However, it partly suffers from the edge-effects (Fang et al., 2009b). The edge effect occurs due to the thermal short-circuit around the edges. This caused because of using high thermal conductive edge sealing made from indium alloy, as example, with thermal conductivity around 83.7 $Wm^{-2}K^{-1}$(Fang et al., 2014). The edge effect is inversely proportional to the size of glazed window that's why the center-of-pane U-value is lower than the total glazing U-value (Eames, 2008). Due to the complexity of achieving the hermetic-edge seal (Memon et al., 2015; Zhao et al., 2007), the construction cost of vacuum glazing still a big issues.

Table 1 summarizes the recent investigations related to enhancing the insulation performance of the VG. The table gives information about the recent VG dimensions, research direction and conclusions. Among these investigations, some points can be concluded. First, the thermal bridge through the sealing material increases with the increase in the sealing edge width and with decreasing the glazing dimensions. This mean that the U-value for the small windows increases because of the edge sealing. Second, the common investigated sizes of the VG ranging from small sizes of 0.2 m × 0.2 m to 1 m × 1 m. Third, the common vacuum gap thickness is attained by the support pillars with height ranging from 0.12 to 1 mm. Forth, keeping the vacuum for a long lifetime and decreasing the manufacturing process and cost are crucial issues facing the VG manufacturing (Chuntonov et al., 2018). Finally, the 3D model is more accurate for estimating the U-value for the VG. In addition, finite volume model (FVM) for analyzing the VG thermal performance is not commonly found in the literature. Therefore, a common VG sample with the commercial dimensions, sealing material, glazing size, and pillars is selected to be compared with a new translucent vacuum insulation panel (TVIP) to overcome the problems that VG faces.

The conventional vacuum insulation panels (VIP) consists of an aluminum gas barrier film with opaque characteristics and solid core thermal insulating material, which is usually kept inside this gas barrier film and thermally sealed after evacuation (Alam et al., 2014). These VIP have lower thermal conductivity ranges from 0.004 $Wm^{-1}K^{-1}$ in immaculate conditions to conventional 0.008 $Wm^{-1}K^{-1}$ (Kalnæs and Jelle, 2014). The inner core material of the VIP is usually constructed with an evacuated solid porous-core material such as fumed silica (Alam et al., 2014), polycarbonates (Kwon et al., 2011), phenolic foam (Kim et al., 2012), glass fibres (Di et al., 2013), and/or fibrous powder (Mukhopadhyaya et al., 2009). The aluminum gas barrier envelope maintains vacuum pressure of up to10 Pa (Choi et al., 2016) and minimizes the heat transfer by gaseous molecules and water vapors through outside cover. This kind of super insulating material is commonly applied in the exterior surfaces of the buildings with different thickness (Wang et al., 2015). Due to the non-transparent nature of the conventional VIP, it cannot be applied for windows due to the window transparency requirements.

The VIP sealing is completely easier than the VG. No sealing material is required. Thermal sealing are most common. In addition, to ensure vacuum stability, two layers of gas barrier films (Jung et al., 2014) with getter adsorption material were used (Yang et al., 2018). Further, the inner core material normally has a larger thickness sometimes around 20 mm. This core material is fabricated from low thermal conductivity material. This mean that the heat loss through the VIP still very low even with a slight increase in the vacuum pressure. These advantages encourage the researcher to find a new transparent vacuum insulation panel (TVIP) to be attached for the glazing's facades. This kind of TVIP could also be easier to the retrofitting options for the existing buildings. Therefore, to keep the VIP transparent, a transparent gas barrier film must be used. In addition, the core material itself must be hollow or structured core as appear in this work for the first time in comparison with VG.

In this paper, an idea at which the possibility of making VIP translucent or semi-transparent has made it possible to compare its ther-

Table 1
Summary of the recent VG investigations.

(Authors, year)	Study*		Aim of the study	Detailed dimensions of the VG components (mm)**				Simulation model	Findings
	Exp.	Th.		Vacuum gap	Glazing's Length / Width/ Thickness	Pillar diameter /spacing	Edge sealing width		
(Zhu et al., 2020)	–	✓	The effect of edge sealing width, glass layer thickness, width of insulation frame, pillars spacing, and pillar material on the performance insulation of the VG is numerically investigated.	0.15	300–1000/ 300–1000/ 2–6	0.4/ from 30 to 50	10	FEM, ANSYS, 3D	1- The U-value linearly increases with increasing the substrate glass thickness, and the larger glazing size, the lower the increasing rate. For VG with size larger than 1 m × 1 m, the U-value hardly changes with the glass thickness. The U-value of the VG decreases linearly with decreasing in the sealing edge width. Increasing the support pillar spacing and decreasing the thermal conductivity of the support pillars decreases the U-value. Including a glazing frame effectively decreases the total glazing's U-value. The thermal insulation frame does not affect the center of pane temperature.
(Fang and Arya, 2019)	–	✓	Tempered glass is used in VG to reduce the number of the support pillars in the evacuated glazing. Because the tempered glass is 4 to 10 times stronger in the mechanical structure compared with the traditional annealed glass.	0.15	400/400/4 And 1000/ 1000/4	0.4/50	6	FEM using ABAQUS, 3D	1- The U-value of the VG with emittance of 0.03 is 0.3 and 0.57 $Wm^{-2}K^{-1}$, for tempered glass and annealed glass respectively. This is due to a reduction in the number of the support pillars, leading to reduction in thermal conduction bridge through the through pillars. Increasing the glazing's dimensions from 0.4 × 0.4 m^2 to 1 × 1 m^2 decrease the total glazing's U-value from 0.57 to 0.4 $Wm^{-2}K^{-1}$ and from 0.69 to 0.52 $Wm^{-2}K^{-1}$ for the tempered and annealed glass respectively. Due to decrease in the heat conduction through edge seal. The center of pane U-value is lower than the total glazing U-value for both glazing's.

(Son and Song, 2019)	–	✓	2D thermal and stress analysis were conducted to investigate the effect of various geometrical parameters on the U-value and concentration of stress caused by the pillars.	0.25–1	200/300/3	From 0.4 to 1/ From 10–40	0.4	FEM, ABAQUS, 2D	1- Stress concentration caused by Hertz contact may cause fracture in the glass panes. They recommended three spacers to avoid this. They recommended to add an elastomer layer between the glass and the pillars to avoid such fracture in the VG.

Table 1 (*Continued*)

(Authors, year)	Study*		Aim of the study	Detailed dimensions of the VG components (mm)**				Simulation model	Findings
	Exp.	Th.		Vacuum gap	Glazing's Length / Width/ Thickness	Pillar diameter /spacing	Edge sealing width		
(Memon, 2017)	✓	✓	Cerasolzer CS186 alloy with J-B Weld epoxy-steel resin were examined for edge sealing of the VG.	0.15	300/300/4	0.3/24	10	FEM	1- The center-of-pane and total glazing U-value of the manufactured triple VG are around 0.33 W m^{-2} K^{-1} and 1.05 W m^{-2} K^{-1}, respectively.
(Ghosh et al., 2016)	✓	–	Outdoor evaluation of thermal and daylight performance of a VG sample was determined in a clear and sunny day, intermittent day and overcast days.	0.2	350/200/3	20	NA	NA	1- The VG average U-value was 1.4 W/m^2 K. Solar heat gain coefficient of VG sample varied between 0.58 and 0.19. The VG reduce 53% heat loss compared to double-glazing for the same area with nearly equal heat gain. The internal daylight was very slightly affected because of fine pillars.
(Fang et al., 2009a)	✓	✓	Thermal cycling test was undertaken. The air temperature on one side of the sample is kept at 22 °C while the other side air temperature changed from −30 °C to + 50 °C and back to −30 °C for 15 times.	0.15	400/400/4	0.4/25	6	FEM, ABAQUS, 3D	1- It was concluded that before the cycling test, the lateral heat conduction account for more than 1/3 of the total heat flow in the VG. However, after thermal cycling, lateral heat flow contributes to less than 1/3 of the total heat flow for the vacuum glazing because part of heat flows through the residual gas. The vacuum pressure within the vacuum gap increased from the negligible level (less than 0.1 Pa) to 0.16 Pa.
(Fang et al., 2009b)	✓	✓	A 2D and 3D model is developed for the VG sample. In the 3D model	0.12	400/400/4 and 1000/ 1000/4	0.4/25	6	FEM, 2D and 3D	1- The predicted difference in the estimated U-value between the 2D and the 3D models for the VG was less than 3%.

* (Th : theoretical; Exp.: Experimental); ** (NA : not available or mentioned in the research work).

mal performance with VG. Therefore, the novelty of this study is based on three main aspects. First, a new structured-core translucent vacuum insulation panel (TVIP) is designed and developed to innovate the VIP and making it possible to resolve the complexity of the edge seal and subsequent construction cost issues that VG faces. In addition, the proposed TVIP can be attached as fixed curtains for the windows of already built dwellings by attachment to the existing glazing. The TVIP proposed in this study differs from the metalized film VIP. It is manufactured from hollow polycarbonate frame encapsulated in a translucent multilayered polymeric envelope to keep the panel element semi-transparent. Second, the thermal transmittance (U-value) under ASTM boundary conditions is performed for both VG and TVIP at different vacuum pressures and window sizes. This section gives a complete guidance for the practicability of each insulation method based on

the window sizes and its achievable vacuum pressures. In addition, it elucidates the effect of vacuum deterioration on the insulation performance of both systems. Third, a detailed 3D finite-volume (FV) heat transfer model is developed and validated to conduct this comparison. This model concurrently solves the heat transfer mechanisms in vacuum insulation systems. The model is very sensitive to core structure design, vacuum gas conduction, and surface to surface radiation. The model is validated with the experiments in this work and with the numerical finite element model (FEM) reported in the literature. Estimation of U-value and cost analysis were conducted for both VG and TVIP systems per square meter of the unit.

Hence, the aim of this work is to computationally compares two different insulating methods. Each method has its own dimensions, design, and manufacturing steps. These dimensions were defined based on the structure design for each insulating method as given in (Fischer-Cripps et al., 1995) for VG and in the authors' earlier work (Yang et al., 2018, 2017) for TVIP. These structure analyses were used to define the detailed dimensions to keep the vacuum gap without glazing fracture because of the high vacuum loads. Both the VG and TVIP were proposed for glazing thermal insulation. However, a compression between the thermal performance analysis and the cost analysis of these two different insulation systems at different glazing sizes and different vacuum pressure were not appeared anywhere in the literature.

2. Design and construction of TVIP in comparison to VG

Typical VIPs are covered with aluminium envelope that restrict innovating VIP to be semi-transparent and cannot be suitable to replace conventional windows. Vacuum glazing is slim and transparent but incorporates higher construction cost (Memon et al., 2019) and effects of thermal short-circuit across the edges. Therefore, in this paper an attempt of designing the translucent or semi-transparent vacuum insulation panel (TVIP) is made in comparison to the vacuum glazing (VG) as shown in Fig. 1. The first method, Fig. 1(a), typical VG, in which two panes of glass separated by support pillars having the vacuum space sealed around the edges with the edge-sealing material of indium alloy. The other method, as shown in Fig. 1(b), is a new structured core with translucent barrier based vacuum insulation panel is attached to the window of the existing buildings. This study compares the thermal insulation performance of these two methods at different sizes of glazing and at different vacuum pressure.

Fig. 2(a) show the detailed structure of VG with single layer of vacuum. In this structure, a very small vacuum layer at the height of 0.12 mm is kept in between two 4 mm thick panes of glass. To keep this vacuum space, an array of very fine support pillars made of stainless-steel is used and uniformly spaced with 25 mm between every two pillars. The distance between these pillars are optimized based on the structure analysis conducted in the literature (Wilson et al., 1998). Stainless steel pillars with a diameter of 0.4 mm is used (Griffiths et al., 2006). To keep the vacuum for a very long period, the edges around the glass sheets must be hermitically sealed. In this work, indium metal sealing with width of 6 mm is used (Fang et al., 2014). These dimensions are kept constant during the comparison for all the finite-volume modelling cases. In this study, a square glazing, $L_p = W_p$, is used with different sizes of 15 cm, 20 cm, 30 cm, 40 cm, 60 cm, 80 cm, and 100 cm. At high vacuum pressure, the heat transfer by gas convection can be neglected and the gas conduction is decreased. The radiation exchange is the most dominant factor in the VG technology at very high vacuum pressure. Therefore, the two glass panes were coated with low-emissive coating of 0.18 to decrease the radiation heat exchange between the two glass panes.

On the other hand, this work introduces another option for the thermal insulation for glazing. In this method, a non-traditional translucent vacuum insulation panel (TVIP) is manufactured with different trial production methods (Katsura et al., 2019). This panel differs from the traditional VIP. In the traditional VIPs, solid core structure with opaque metalized gas barrier film is used. This kind of VIPs are used to accomplish thermal insulation for the walls with opaque characteristics. However, the current VIP has transparent gas barrier film with hollow structured core polycarbonate material to keep the vacuum. This panel is attached to the glass layers of the windows of the existing buildings as curtains. Therefore, retrofitting option can be easily accomplished. In more details, the structure and dimensions of this design is depicted in Fig. 2(b). It consists of a new 3D printed polymeric frame. In this structured core frame, the dimensions of the vacuum spacing, D and thickness were defined based on the structure analysis developed by (Yang et al., 2017). To decrease the heat exchange between the two sides of vacuum space, a low emissive film with emissivity of 0.28 is used on one side of the VIP. Further, to keep the vacuum inside the structure for a long time, a sealed edge is thermally performed as detailed in later sections. These TVIPs are constructed in this paper with the required dimensions and attached to the existing single layered glass windows. The layer structure and thicknesses of the translucent gas barrier film used in the TVIP is depicted in Fig. 2(c), it shows the air transmission rate, moisture transmission rate, and heat seal strength. These parameters are essential for the simulation of the stability of the vacuum pressure and its ageing effects.

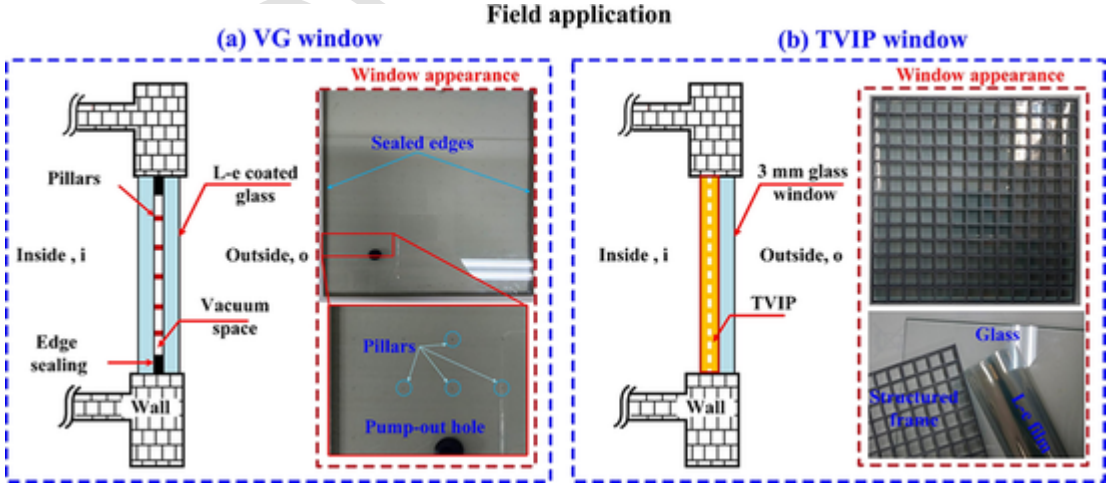

Fig. 1. Schematic diagram detailing the real field application of (a) Vacuum glazing (VG) and (b) proposed translucent vacuum insulation panel (TVIP) as a replacement to glazed window.

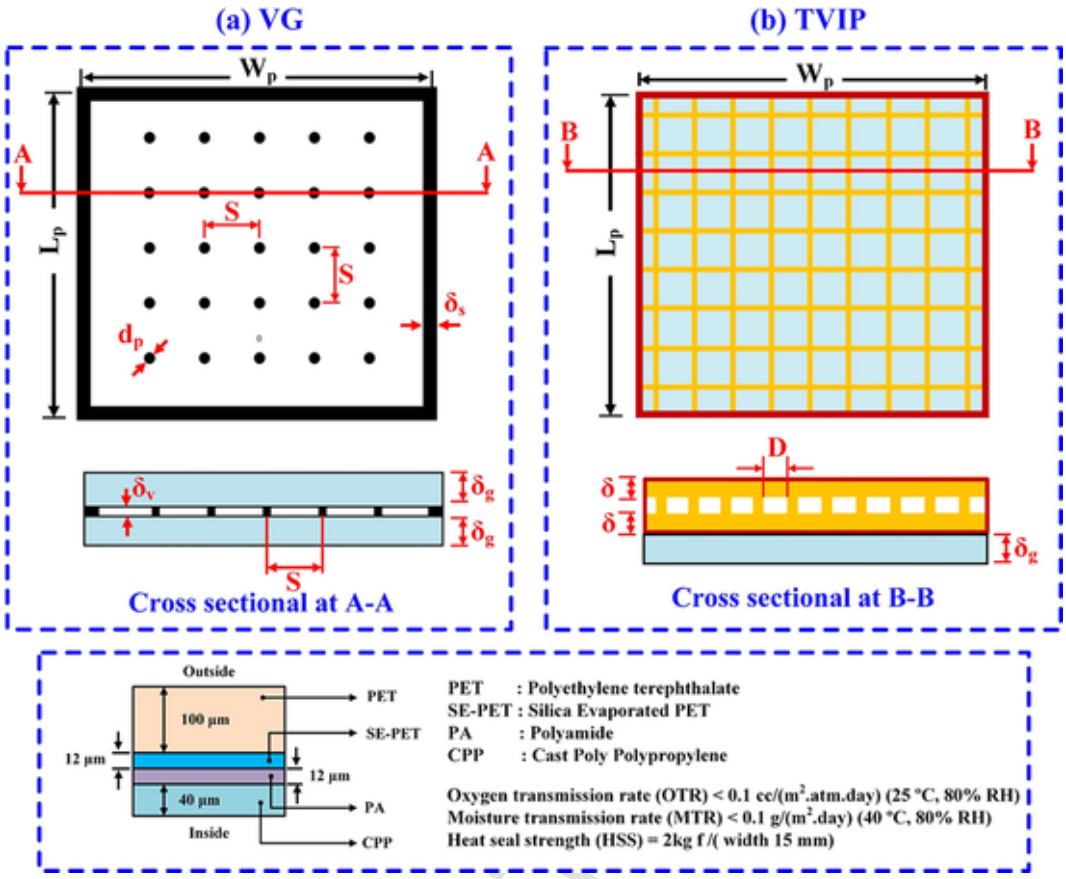

Fig. 2. Detailed structure of (a) VG, (b) TVIP glazing, and (c) structure of the transparent gas barrier film used in the TVIP.

2.1. Experimental setup

The experimental setup in this paper is only used for estimating the centre of pane thermal conductivity. The measured value is used to validate the numerical finite-volume model which is then used to extend the study at different vacuum pressure and glazing sizes thermal performance. The experimental setup developed for this paper is a cost-effective method by saving the material consumption in experiments. The experiment starts with sample construction, and then followed with thermal conductivity measurements.

In VG sample, the construction steps, displayed in Fig. 3(a), were started with cleaning the two panes of glass using water followed by acetone and then drying using oven at the temperature of 120 °C. Then, pump-out hole with 2 mm diameter is drilled for the purpose of evacuation. This hole is located at 75 mm from the corner of the glazing. A 6 mm wide layer of indium layer was soldered around the periphery on the coated sides of both glass panes. The support pillars were located on the lower glass pane using a vacuum wand. To accomplish a very fine vacuum space in the VG sample, an array of very fine stainless-steel support pillars with height of 0.12 mm is placed on one glass pane and uniformly spaced with 25 mm between every two pillars. And by placing the other top glazing layer, the vacuum layer with a vacuum thickness equal to the pillar's height can be accomplished (Fang et al., 2014). Then the sample was heated up to 2 h in oven to join the two panes of glass. Further, steel reinforced epoxy was used around the panel edges to enhance the mechanical stability of the main edge seal. After that, the sample was placed on hot plate to allow the pane heating during the evacuation. The evacuation is simultaneously performed during the heating using the vacuum system with the use of vacuum cup as show in Fig. 4(a). After reaching the desired vacuum pressure, the pump-out hole was sealed using the vacuum cup which has a cartridge heater to melt the sealing material fixed inside it.

On the other hand, the TVIP is constructed following the steps in Fig. 3(b). These steps start with keeping the TVIP materials inside oven at temperature of 70 °C for 24 h. This allow releasing the outgassing's from the structure materials of the VIP. Then the frame structure with the low emissive film are kept inside three-sided sealed transparent envelope. Three edges of the envelope were sealed using vacuum sealing machine with thermal sealing width of 8 mm. And low-emissive film used in this work has emissivity of 0.28 and 0.77 for its faces. The lower emissivity is kept towards the vacuum space. The frame structure and the low-emissive film were put in the gas barrier envelope. Then the full structure is evacuated and after reaching the vacuum pressure using the evacuation system shown in Fig. 4(b). During the evacuation, the thermal conductivity of the TVIP sample is measured to be used for the numerical model validation. Commercially, indium edge sealing is mostly used in the VG. This sealing material has a thermal conductivity of $87.3 Wm^{-1}K^{-1}$. This significantly contribute to increasing the glazing U-value specially at lower sizes of the glazing. Therefore, in the new design of the TVIP, transparent gas barrier film is used to hold its components. In addition, thermal edge sealing is performed.

After the successful construction of VG sample, the thermal conductivity measurements were conducted using the schematic representation in Fig. 4(c). In Fig. 4(c), heat flow meter (HFM) apparatus is shown and is used to measure the centre of pane thermal conductivity of VG and TVIP samples. The thermal conductivity of the sample is measured based on the following equation given in the manufacturing datasheet: -

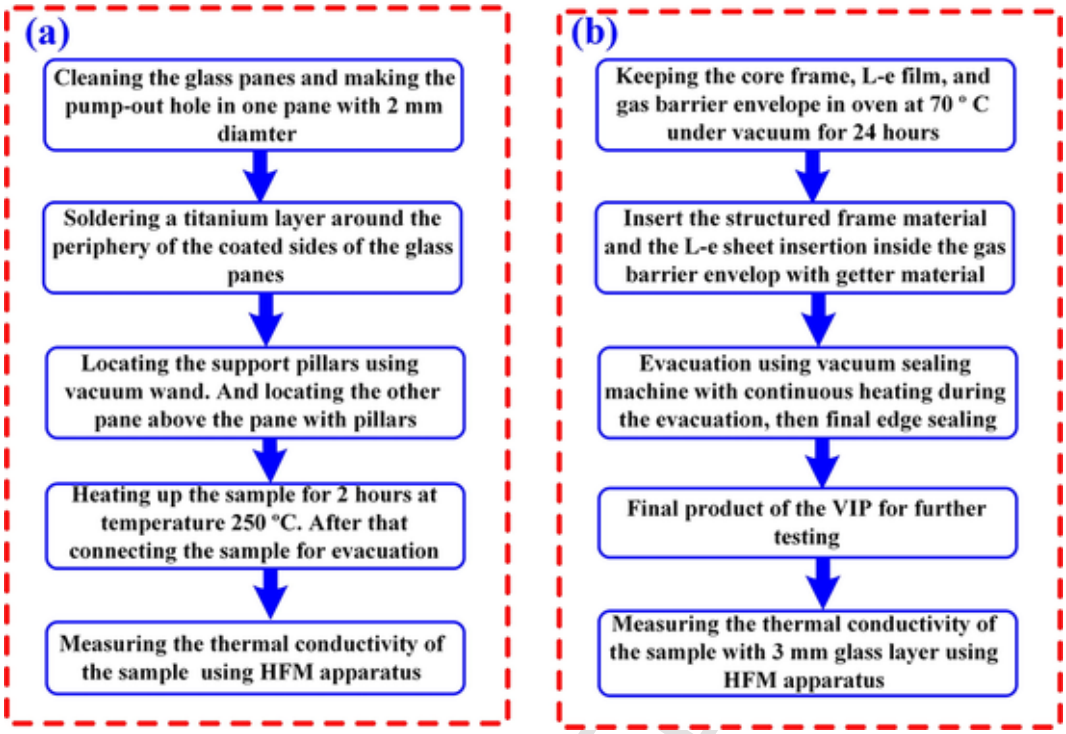

Fig. 3. Detailed construction steps of (a) VG and (b) TVIP glazing.

$$k_{sample} = \left(\frac{q_h + q_c}{2}\right) \times \frac{Samplethickness}{\Delta T} \quad (1)$$

where; k_{sample}, q_h, q_c, ΔT are the pane thermal conductivity in ($Wm^{-1}K^{-1}$), heat fluxes measured by two heat flux sensors one the hot and the other on the cold sides of the sample in (Wm^{-2}), and controlled temperature difference on the sample sides. The HFM apparatus has the facility to measure these parameters by controlling the temperatures of the hot and cold side of the sample along with the sample thickness with high accuracy. For the HFM apparatus, the maximum width of the sample must not exceed 20 cm. Therefore, the experimental samples were manufactured with dimensions of 20 cm by 40 cm for the VG and 15 cm by 15 cm for TVIP sample. Then the numerical model is validated with the experimental results for these dimensions and then analysis was conducted by increasing the dimensions of the samples by the numerical simulation. The detailed dimensions of the compared samples are depicted in Table2.

2.2. Theoretical analysis

In vacuum glazing technology, the vacuum pressure must be below 0.1 Pa. Due to ageing effect or degradation, an increase of vacuum pressure increases the sample thermal conductivity. Further, the heat transfer mechanisms in vacuum technologies depends on decreasing the gas convection effect. The heat transfer mechanisms in the vacuum devices can be divided into four portions. The first portion is radiation heat exchange between the cold and hot side of the vacuum region through the vacuum space. The second and third portions are the heat conduction through the skeleton of the core structure, and through the gas conduction. And fourth, the heat transfer through the gas convection (Baetens et al., 2010). To improve the insulation capabilities of the vacuum insulation system, all these portions must be decreased. However, at high vacuum level, the mean-free path between the gas molecules increases at least 100 times than the vacuum gap size and can be disregarded in the calculation (Arya et al., 2018; Kwon et al., 2009). Hence, the current problem contains a coupled conduction radiation heat transfer. The 3D heat conduction equation for the solid regions including the glass panes, pillars, and edge sealing for the VG and frame with the glass layer with 3 mm in TVIP were coupled with the surface to surface radiation model. The current model adopt the following assumptions:-

a) Steady state thermal analysis is conducted.
b) The gas convection effect can be neglected within the simulated vacuum pressure (Arya et al., 2018).
c) The thickness of the Low-emissive films is not considered in the conduction heat transfer due to the smaller thickness. However, it's very low emissivity is considered in the radiation exchange which is a dominant factor.
d) The heat conduction through the very thin envelope of the TVIP is neglected.
e) The thermal contact resistances between each layer in the VG and TVIP structure is not considered.
f) The materials are assumed isotropic with uniform thermal conductivity in all the directions.

For steady state 3D heat conduction with radiation source term, ANSYS FLUENT solves the energy equation as follows ("ANSYS FLUENT Theory Guide," 2011):-

$$\nabla.(k\nabla T) + S = 0 \quad (2)$$

where; T is the element temperature, k is the element thermal conductivity, and S is a source term. This term is added to consider the effect of the radiation exchange in the vacuum space ("ANSYS FLUENT Theory Guide," 2011). This equation is also solved for the solid regions in the computational domain but without radiation heat source. Further, in some of the recent investigations, it is assumed that the gas conduction effect can also be neglected at very high-vacuum pressure. However, to include this parameter in the current calculations, the gas thermal conductivity is considered as a function of the pressure, tem-

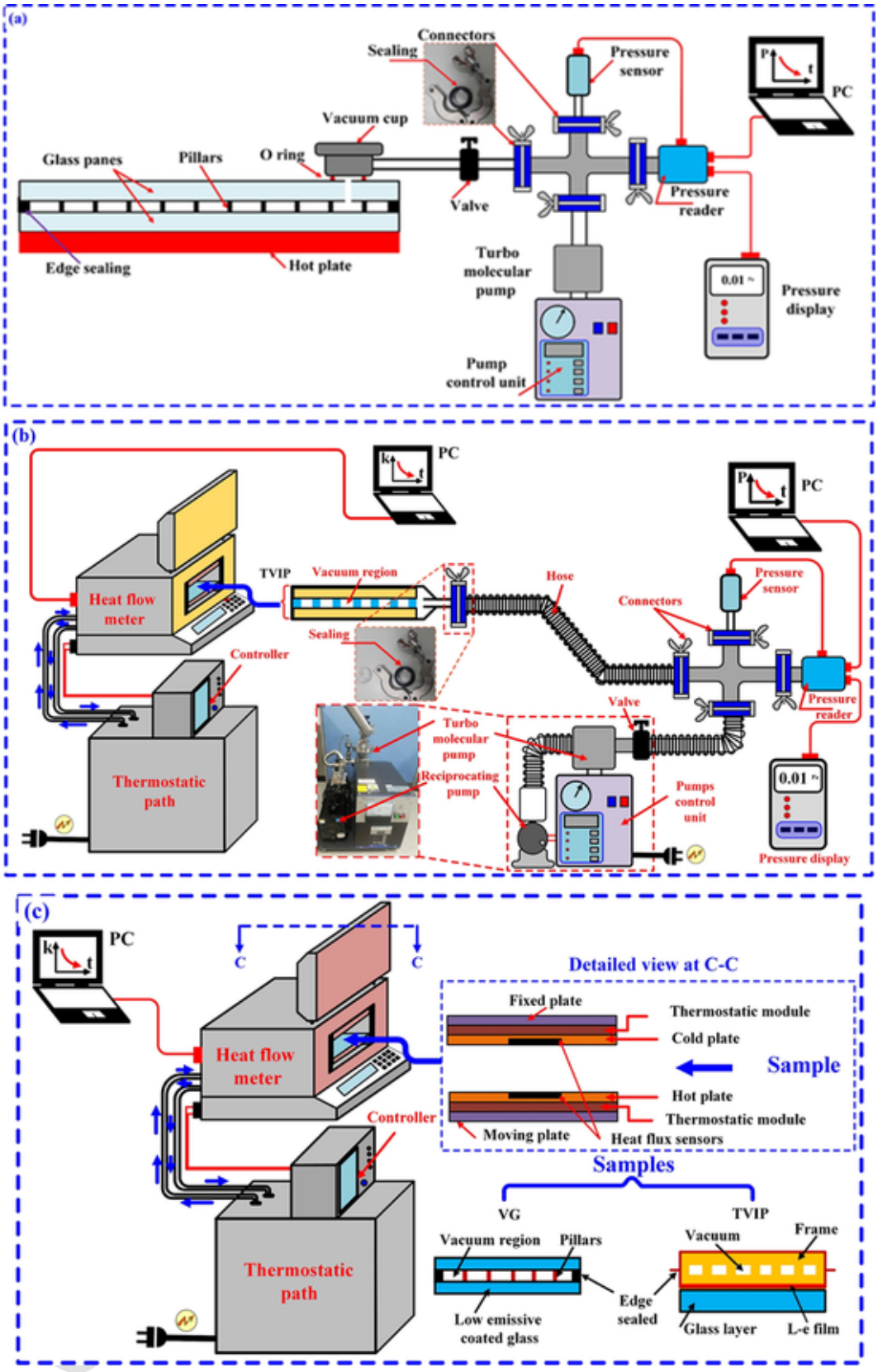

Fig. 4. Detailed experimental setup used for (a) evacuating the VG, (b) evacuating of TVIP with thermal conductivity measurement, and (c) HFM apparatus for measuring the samples thermal conductivity.

Table 2
Dimensions of the VG and TVIP sample.

Sample	Dimension	Value (mm)	Dimension	Value (mm)
VG	S	25	d_p	0.4
	δ_s	6	δ_v	0.12
	δ_g	4	δ_{VG}	8.12
TVIP	Δ	1	δ_{TVIP}	6.33
	δ_g	3	D	8
The length and width		$L_p = W_p$ = 15, 20, 30, 40, 60, 80, and 100 cm		

perature, and vacuum thickness (Kim and Song, 2013). However, to neglect gaseous conduction, the gas pressure must be less than 0.1 Pa. In this work, the air thermal conductivity in the vacuum space at different pressure, temperature and pore size is calculated as follows:

$$k_v = \frac{k_o}{1 + \frac{(1.07\times10^{-7})T}{l_v P}} \quad (3)$$

where T, l_v, and P are the gas temperature in K, vacuum layer thickness in m this values are 0.00012 m and 0.003 m for VG and TVIP system respectively, and gas pressure in Pa respectively. In addition, k_o is the air thermal conductivity at the room temperature and pressure which is about 0.026 W/m. K.

To predict the radiation effect in the VG and TVIP, coupling the heat conduction with the surface to surface (S-S) radiation is accomplished using commercial software ANSYS. This model defines all the faces contributing in the surface to surface radiation and calculates the view factor these surfaces. The surfaces contributing in the radiation were the surfaces in direct connection to the vacuum regions ("ANSYS FLUENT Theory Guide," 2011). The radiation energy exchange these surfaces depends on their size, separation, and orientation. These parameters were used to estimate the view factor between these surfaces. It was calculated using ANSYS fluent the coordinates of these surfaces from the design geometry. Therefore, the essential parameters to estimate the view factor were defined based on the design geometry of the vacuum device. The details, limitations of S-S radiation model can be found in ANSYS theory guide ("ANSYS FLUENT Theory Guide," 2011). The computational domain used in the current simulation is the full scale of VG and TVIP window as depicted in Fig. 5(a) and (b) respectively. The thermal conductivity of each layer in the VG and TVIP window are summarized in Table 3.

2.3. Boundary conditions

In this study, ASTM standards for winter conditions were used through the full simulation work of this paper as recommended by (Fang et al., 2009b). In these boundary conditions, the indoor and outdoor ambient air temperatures were assumed constant at 21.1 °C and −17.8 °C respectively (Memon et al., 2019). In addition, the convective heat transfer coefficients on the inside and the outside surfaces of the window were set to be 8.3 and 30 $Wm^{-2}K^{-1}$ respectively. In more details, in the VG, the outside boundary conditions are defined as convective boundary with the ASTM conditions. However, to include the effect of the Low-emissive coating, the emissivity of the interior glass walls in contact with the vacuum region is defined to be 0.18 for VG on both sides of glass panes. However, it is defined by 0.28 for one side in the TVIP window. This because only one sheet of Low-emissive film is used on one side near the hot side of the TVIP. Further, the peripheral sides of the VG and TVIP are assumed to be adiabatic due to the smaller thickness of the panes compared with the surface area. The thermally coupled boundary conditions is used at all interfaces. In this case, the temperature on these interfaces and the heat transfer rate is the same. Mesh independent test is performed to confirm that the results are independent on the number of elements. The number of elements used for the simulation changes according to the computational domain size. For instance, it is noticed that for 15 cm × 15 cm window, a total number of elements of 2,964,263 and 1,038,336 are used for the simulation of the VG and TVIP window respectively. The mesh details for the VG and TVIP are illustrated in Fig. 6(a) and (b), respectively.

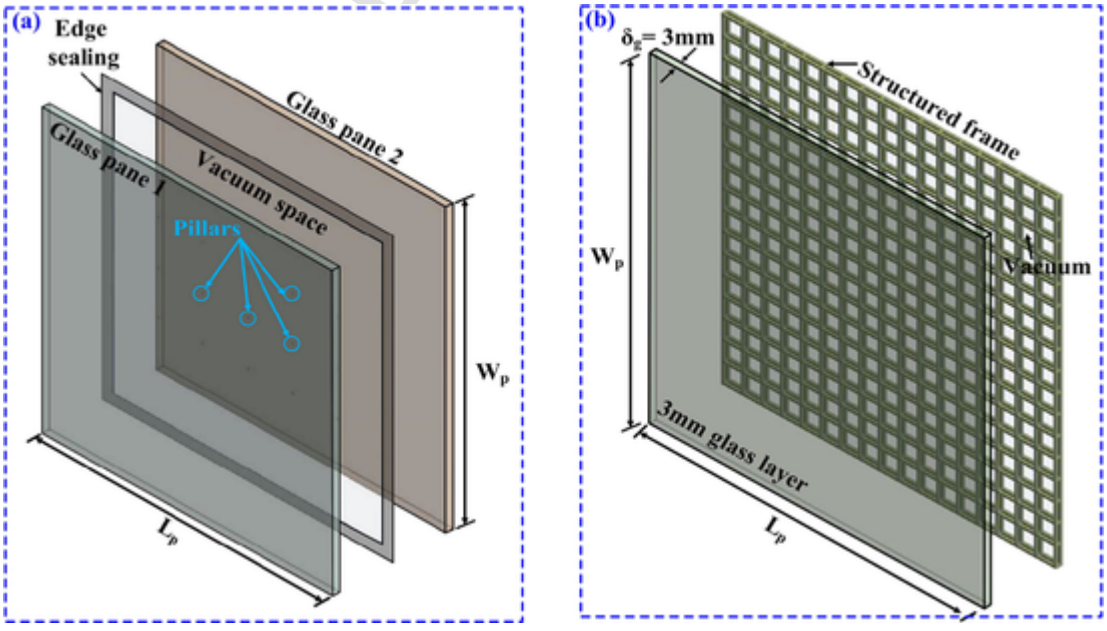

Fig. 5. Computational domain layers of (a) VG, and (b) TVIP, (note: the computational domain displayed in a separated parts to show the detailed structure, but these parts are connected in the simulations).

Table 3
Thermal conductivities of the layers used in the simulation.

Glazing type	Material	Thermal conductivity
VG	Coated glass pane	1 $Wm^{-1}K^{-1}$
	Pillars	20 $Wm^{-1}K^{-1}$
	Sealing material	83.7 $Wm^{-1}K^{-1}$
TVIP	3 mm glass pane	1 $Wm^{-1}K^{-1}$
	Frame structure	0.2 $Wm^{-1}K^{-1}$

2.4. Numerical methods

This simulation work is conducted, using a licensed version of ANSYS 19.2. In this simulation, surface to surface radiation model, S-S model, is activated. The solution steps started with creating the 3D computational domain with the full scale. This step is performed using DesignModular tool. In this step, multizone approach is used. In multizone approach, the computational domain is separated into several zones to enable us to control the meshing, properties, and the boundary conditions of each zone separately. This idea is very efficient for the applications with very fine zones in large computational domains like very fine pillars with 0.12 mm height in a large domain with 1 m by 1 m area. Then, the interfaces between each zone and the adjacent zones were thermally coupled. This enable sharing the temperatures and heat fluxes on these interfaces. After that, the computational domain was divided into several elements in the meshing tool. This step is performed by defining the element size, and element shape. The mesh details for both VG and TVIP is displayed in Fig. 6(a) and (b) respectively. Then, the generated mesh is exported to Fluent solver. In Fluent, the heat flow equations including continuity, and momentums and energy equations are implemented. However, in this simulation no flow equations exists due to the convection neglection. Therefore, the flow equations are deactivated (Memon et al., 2015; Memon and Eames, 2017). Only the energy equation is solved for the current problem. However, to activate the S-S radiations model, fluid zone must exist. Therefore, the vacuum space is modeled as a fluid zone, but with deactivating the flow equations. To use the S-S radiation model, estimating the view factor between the participating surfaces must be done. So, from the imported computational domain, S-S model evaluates the orientation, areas, and spacing of all the face participating in the radiation. These parameters are used for the calculation of the view factors. The energy equation for both the solid regions and the vacuum region with radiation were simultaneously solved. And the radiosity estimation is achieved based on the estimated view factors. The solution is continued until the residual in the radiosity and the energy equation reached 10^{-6} and 10^{-13} respectively.

2.5. Model validation

The current model is validated by using two sets of results. First, the current model results were compared with the experimental results conducted in this study as presented in Section 2.5.1. The second validation step is conducted by comparing the current predicted results with the numerical data in two recent investigations of (Fang et al., 2009b) and (Zhu et al., 2020). And these comparisons were presented in Section 2.5.2.

2.5.1. Validation with experiments

In Fig. 7-a, the measured thermal conductivity of the VG and TVIP samples were compared with the numerical results obtained from the simulation model. The thermal conductivity of these samples was measured using the HFM apparatus in Fig. 4-b and 4-c for TVIP and VG samples respectively. It is noticed that the measured center-of-pane thermal conductivity of the VG is about 8.6×10^{-3} $Wm^{-1}K^{-1}$ at vacuum pressure of 0.1 Pa. In this experiment, the VG sample consisted of two glass panes 3.2 mm thickness each and 0.12 vacuum gap. Indium sealing with edge sealing width of 6 mm and pillars with dimeter of 0.4 mm were used in the fabrication steps. The VG sample used in the experiment was a rectangular glazing with length and width of 35 cm and 20 cm respectively. Therefore, in the validation step, the model is constructed for the same dimensions as in the experiment. In addition, the measured thermal conductivity of the TVIP sample without the 3 mm glass layer was about 6.8×10^{-3} $Wm^{-1}K^{-1}$ with sample thickness of 3.12 mm at a pressure of 0.2 Pa. The simulated results showed a good agreement with the measured center-of-pane thermal conductivity with values of 8.7×10^{-3} $Wm^{-1}K^{-1}$ and 7.1×10^{-3} $Wm^{-1}K^{-1}$ for VG and TVIP respectively. Th deviation between the experimental and the numerical results is a round 4%.

To further validate the current model with experiments, the fabricated VG and TVIP were tested using hot box calorimeter. During this test, the glazing is set to separate between two different air zones. Each zone has air with certain temperature and convection heat transfer coefficient. The air in one zone is kept at a temperature around 25 °C while the other zone is kept at a temperature around −9 °C. And the heat flux at the center of the panes were measured at the experimental conditions presented in Table 4. The measured values of the center-of-pane heat flux were compared with the numerical predicted results in Fig. 7-b. During the simulation, the boundary conditions used in

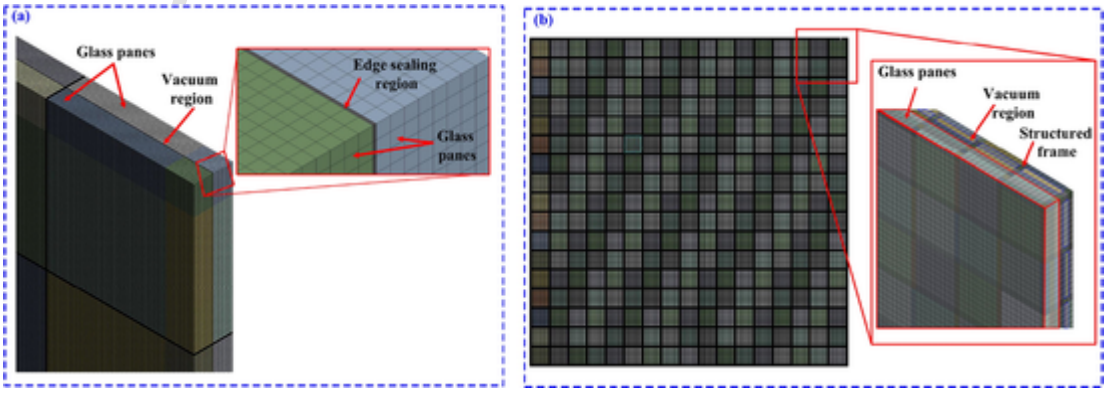

Fig. 6. Three-dimensional finite-volume mesh details of (a) VG and (b) TVIP.

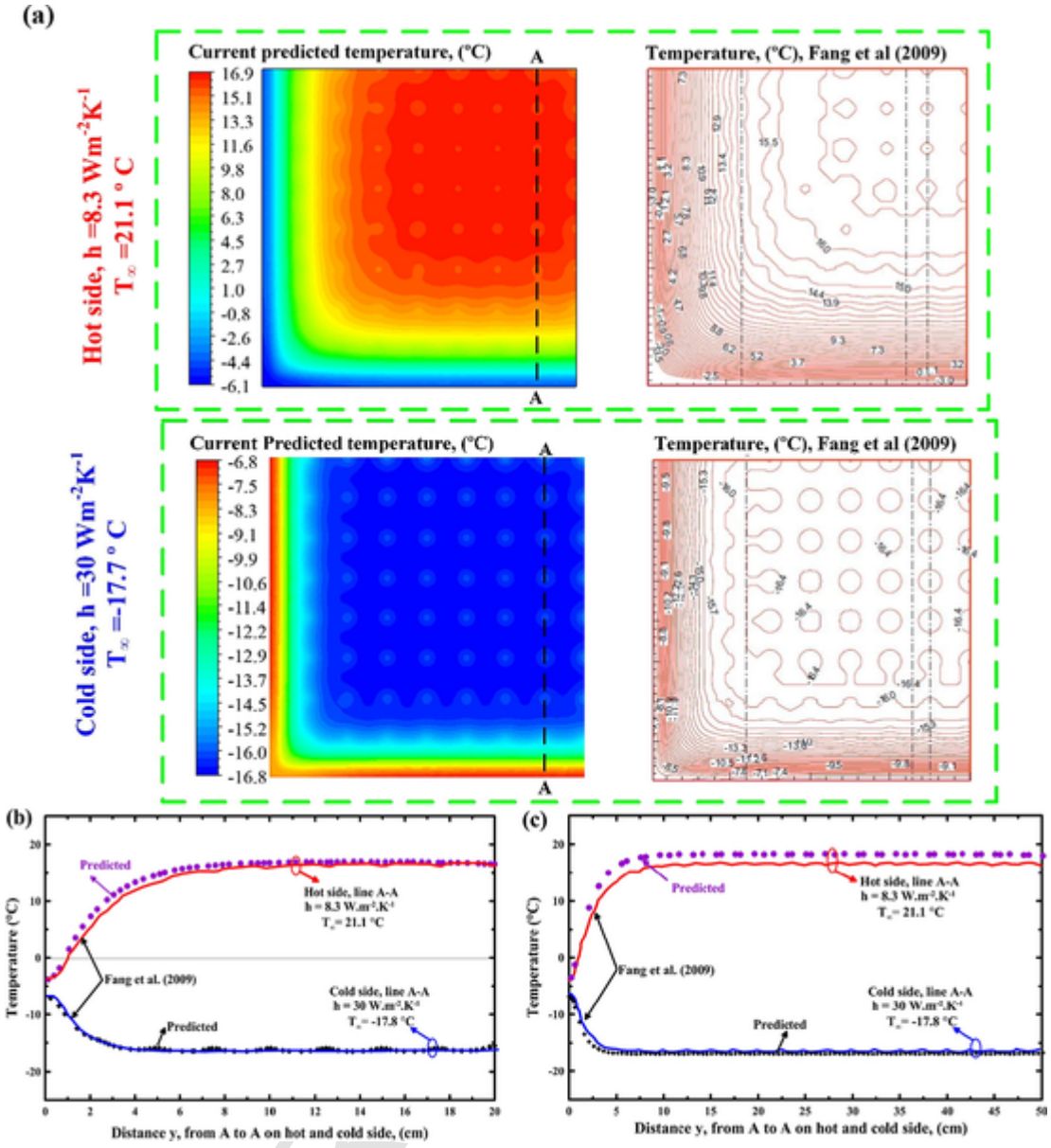

Fig. 7. Comparison between the predicted numerical results and the experimental results of (a) glazing's center-of-pane thermal conductivity and (b) center-of-pane heat flux.

Table 4
Steady state experimental parameters used in the validation step.

Sample	$T_{\infty,in}$(°C)	$T_{\infty,o}$(°C)	$h_{\infty,in}$(W.m $^{-2}$.K $^{-1}$)	$h_{\infty,o}$(W.m $^{-2}$.K $^{-1}$)	q''(W.m $^{-2}$)	Vacuum pressure
VG	−9.08	25.46	18.0	9.0	37.63	0.1 Pa
TVIP	−9.55	25.87	11.7	9.0	79.37	1 Pa

the experiments and mentioned in Table 4 are used instead of ASTM boundary conditions. It is noticed that the model accurately predict the estimated values of the centre of pane heat flux with a maximum error around 2%.

2.5.2. Validation with recent investigations in the literature

Two set of results were used to validate the current model with results of Fang et al., (2009b) and another recent published results in (Zhu et al., 2020). First, the current model is validated by comparing the predicted VG results with the results in (Fang et al., 2009b). The current predicted temperature contours on the cold and hot side of the vacuum glazing window are compared in Fig. 8(a) with the results obtained in (Fang et al., 2009b). In this validation step, two different sizes of VG with dimensions of 40 cm × 40 cm and 100 cm × 100 cm were simulated. During the validation step, the same edge-sealing material, glass thickness, thermal conductivities and pillars dimensions are used as the same as used in (Fang et al., 2009b) for fair comparison. The predicted temperature contours on the hot and cold side of the VG with dimensions of 40 cm × 40 cm were depicted in Fig. 8(a). It is obvious that the same trend of the results are predicted with lower tem-

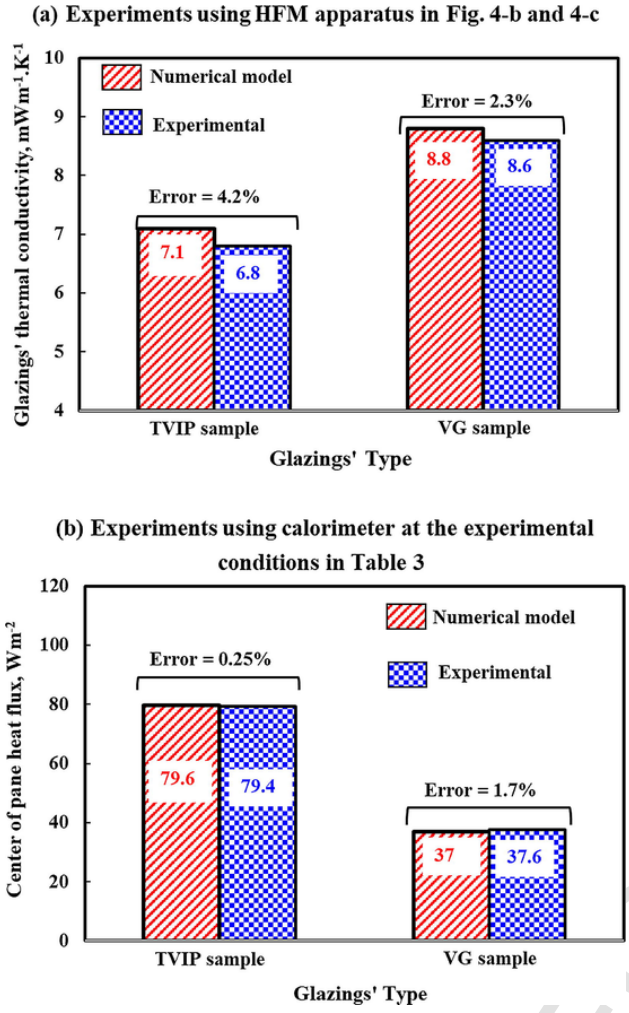

Fig. 8. Three-dimensional finite-volume model validation with the numerical results of Fang et al (2009b) shows (a) temperature contours at the hot and cold side of the VG with dimensions of 40 cm × 40 cm; (b) local temperatures on line A-A at hot and cold sides for VG sample with dimensions of 40 cm × 40 cm, and (b) local temperatures on line A-A for the hot and cold sides for VG sample with dimensions of 100 cm × 100 cm.

perature near the edges on the hot sides and high temperature at the same locations on the cold sides. This is resulted from the edge effect as will be discussed in detail later. Furthermore, to quantitively compare the predicted results with the results of (Fang et al., 2009b) and not relying on the visual basis, the predicted temperature distribution on two lines from A-A on hot and cold sides of VG pane are compared with the same presented by (Fang et al., 2009b). This comparison is conducted for the VG with dimensions of 40 cm × 40 cm and 100 cm × 100 cm in Fig. 8(b) and (c) respectively. From this comparison it is obvious that the current model accurately predict the thermal insulation performance of the vacuum insulation technologies. Quantitively, the relative error is defined as the ratio between the maximum temperature difference between the predicted temperature and the results in (Fang et al., 2009b) to the temperature predicted in (Fang et al., 2009b) at the same location. The temperatures used in degree Celsius. It is found that the maximum relative error is about 8.5% at the hot side of the VG with area of 100 cm × 100 cm this error diminishes with lower size of VG. This difference may be attributed to that the current model considers the estimation of view factors for all interfaces in connection with the vacuum region.

Second, a further validation step is conducted. In this step, the developed model is used to estimate the total glazing U-value for three VG samples with areas of 0.3 × 0.3 m^2, 0.5 × 0.5 m^2, and 1.0 × 1.0 m^2. The comparisons were depicted in Fig. 9. The estimated results from the current model were compared with the estimated results recently published by Zhu et al., (2020). During this validation step, glazing's sizes, material properties, glazing's emissivity and boundary conditions were used as the same as in (Zhu et al., 2020). In more details, the simulation was conducted at a hot side air temperature of 18 °C with free stream convection heat transfer coefficient of 8.7 Wm^{-2} K^{-1}. While the cold side air temperature was kept at −20 °C with free stream convection heat transfer coefficient of 23 Wm^{-2} K^{-1}. The same glazing thickness of 3 mm, vacuum layer gap of 0.15 mm, indium edge sealing with width of 6 mm, and low-emissivity glazing with emissivity of 0.1 were used during the validation. Based on the results depicted in Fig. 9, it is evident that the predicted results are in a good agreement with the results presented in (Zhu et al., 2020) with maximum relative difference of 4.9%. This difference may be attributed to that in this paper, we used the FVM while they used the FEM. The solution methods for both model may cause this slight difference.

3. Results and discussion

This section is divided into three main subsections. In Section 3.1, the effect of changing the vacuum pressure on the local temperature distribution along with the thermal insulation performance of the VG and the new proposed TVIP is discussed. In this section, the vacuum pressure is changed from 0.1 Pa to 10 Pa for small scale glazing with dimensions of 15 cm × 15 cm. The pressure change mimics the vacuum pressure deterioration on the thermal transmittance (U-value) of these two glazing insulation systems. In Section 3.2, the effect of changing the glazing dimensions from 15 cm × 15 cm to 100 cm × 100 cm are discussed and compared. This step is very essential to evaluate the applicability range for both VG and TVIP based on the glazing dimensions. In Section 3.3, the cost analysis is performed for both VG and TVIP.

3.1. Effect of vacuum pressure on the insulation performance of VG and TVIP

In this section, the comparison is conducted under ASTM boundary conditions for a smaller glazing area of 15 cm × 15 cm. To completely understand the detailed thermal insulation performance of VG and TVIP, temperature distributions at different locations along with the temperature contours at different plans are discussed.

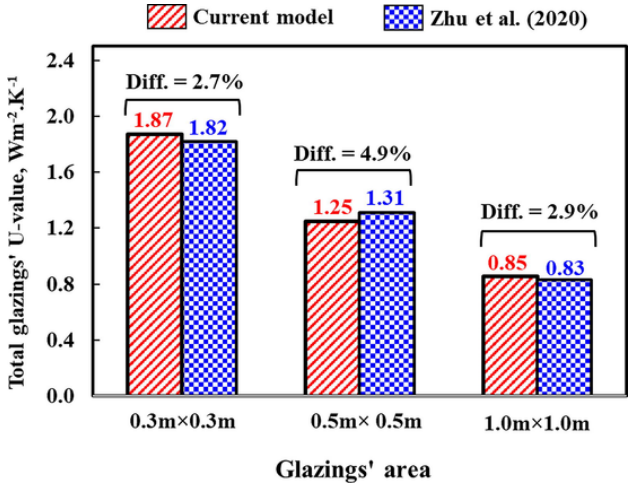

Fig. 9. Comparison of the predicted total gazing U-value for the VG sample at different glazing's areas with the numerical results in (Zhu et al., 2020) using FEM.

3.1.1. Vacuum glazing (VG)

Fig. 10 shows different locations where the temperatures were obtained. First, the location of line A-A is located on both the hot, plane (1), and cold side, plane (3), of the window. This line locates at the mid of the window as seen in Fig. 10. The temperatures on these lines highlights the effect of edge sealing on the thermal insulation performance of the VG. The temperatures at different two locations B-B and C-C are also illustrated in Fig. 10. Line B-B passes through the two glass panes with pillar at the center of the VG whilst the line C-C passes through the two glass panes and the nearest vacuum region at the VG center. The temperatures on these two lines highlight the effect of thermal bridge caused by the pillars compared with the vacuum region. Furthermore, the temperature contours at four planes were also obtained. The first plane, plane (1), locates at the hot side of the window facing the indoor side of the building. This plane is subjected to convection boundary condition with h = 8.3 $Wm^{-2}K^{-1}$ and $T_{\infty, in}$ = 22.1 °C. The second plane, plane (2), is the Low-emissive coated face of the hot glass pane. Similarly, plane (3) and plane (4) are the outside cold side of the second glass pane with h = 30 $Wm^{-2}K^{-1}$ and $T_{\infty, out}$ = −17.8 °C and Low-emissive coated face of the cold glass pane respectively. The locations of these planes are shown in Fig. 10. The predicted temperatures at A-A, B-B and C-C at different vacuum pressures for VG are shown in Fig. 11(a), (b) and (c) respectively.

In Fig. 11(a), the temperatures at line A-A on the hot side increases with the distance from the sealing edge until it reach a nearly constant value and starts to decrease again at the other edge. In more details, the hot side temperature increases from around −5 °C to 15 °C from the edge of the glazing to the center of pane. This is resulted due to the thermal short-circuit across the edges of VG. Therefore, around 10 cm of the both sides from 15 cm of the glass width were affected by the edge sealing. It leads to decrease the thermal insulation performance. This trend is similar to that in the literature by Memon et al (2015) and Fang et al (2009b). However, one of the new added value here is that decreasing the vacuum pressure increases the hot side temperature and decreases the cold side temperature. This is attributed to that at low pressure, the vacuum region's thermal conductivity is decreased. And therefore, the heat transfer from the hot side to the cold side is decreased. Consequently, higher temperature difference between the hot and cold side of the VG were obtained. Furthermore, the effect of the vacuum pressure increase or deterioration on the hot side is much pronounced compared to the cold side. This because of the higher heat transfer coefficient closer to the cold side which nearly keep the cold side temperature near to the cold temperature in ASTM boundary conditions. It is noticed that the support pillars effect on the temperature distribution appears on both cold and hot sides of the VG at lower vacuum pressure. This effect disappear at the lower vacuum pressure of 10 Pa. Therefore, it is recommended that to capture the pillars effect using thermal imaging, higher vacuum pressure of less than 0.1 Pa inside the vacuum space must be attained.

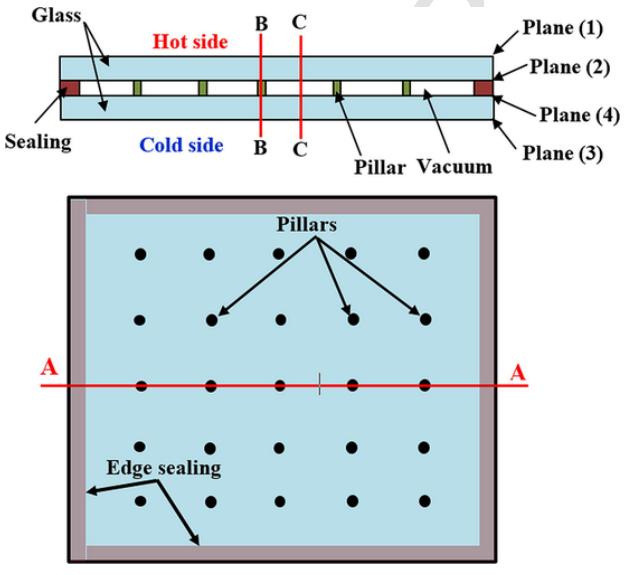

Fig. 10. Location of lines, and planes through the VG.

In Fig. 11(b), the variation of the local temperatures on line B-B passes through the two glass panes with pillar at the center of the VG model is illustrated. The local temperature variation with the VG thickness showed a significant decrease in the temperature occurs through the glass panes while slight temperature decrease occurs through pillars due to the higher thermal conductivity of the pillars with smaller height compared with the larger thickness of the glass panes with lower thermal conductivity. On the other hand, in Fig. 11(c), the temperature variation with the VG thickness through the line C-C is displayed. It is found that the temperature reduction through the glass pane thickness is negligible compared with the temperature difference across the vacuum region although the smaller thickness of the vacuum region. This because the reduction in the radiation effect due to the low-emissive coatings and the decrease in the pressure decreases the vacuum region thermal conductivity. In more details, a temperature difference across the very thin vacuum layer with thickness of 0.12 mm is about 33 °C, 29.2 °C, 16 °C at vacuum pressures of 0.1 Pa, 1 Pa, and 10 Pa respectively.

To further clarify the previous trend, a two-dimensional temperature contours on a plane located at different locations are displayed in Fig. 12 at a vacuum pressure of 0.1 Pa. Plane (1) and plane (2) are used to display the temperatures on the hot surface of the glass pane facing the indoor and the Low-emissive coated side of the hot pane respectively. It is noticed that highest temperatures locates at the middle of the glass pane whilst the lowest values locates at the edges of the glazing with temperature stratification from −5.9 °C to 15 °C. Further, the pillars effect appears at the Low-emissive coated side of the hot glass pane. This illustrates the thermal bridge through the very fine support pillars.

On the other hand, the temperature contours on plane (3) and plane (4) are detailed in Fig. 12. Contradictory to the previous trend of the contours on the hot glass pane is observed. The higher temperatures are observed at the edges while the coldest temperatures occurs at the center of the glass pane. This confirms the same findings of lower heat transfer occurs at the mid of the pane while higher occurs on the edges. Comparing the temperatures contours on plane (1) and plane (3), the effect of the support pillars thermal bridges clearly appears at the cold side compared to the hot side. This is because of the highest heat transfer at the colder side compared with that at the hotter side of the glass panes.

Fig. 13 shows the temperature contours on the hot side of the glass pane, plane (1), at different vacuum pressures. It is noticed that increasing the vacuum pressure or losing the vacuum inside the VG from a pressure of 0.1 Pa–10 Pa decreases the inner glass pane average temperatures from 12.2 °C to 3.8 °C respectively. This means that the higher heat transfer rate from the inside of the building though the glazing could be attained. Further, increasing the vacuum pressure ten times, from 0.1 Pa to 1 Pa, decreases the VG inner hot side temperature by only 1.2 °C. Whilst, increasing the pressure ten times increases the average hot side glass pane temperature by 5.8 °C. This is because of the thermal conductivity of the vacuum region is not a linear relationship with the pressure as seen in Eq. (3).

The temperature contours on the cold side of the VG, plane (3), is displayed in Fig. 14 at different vacuum pressures. It is obvious that increasing the vacuum inside the VG, from 0.1 Pa to1 Pa, increases the average cold side temperatures from −13.8 °C to −13.5 °C. Such incre-

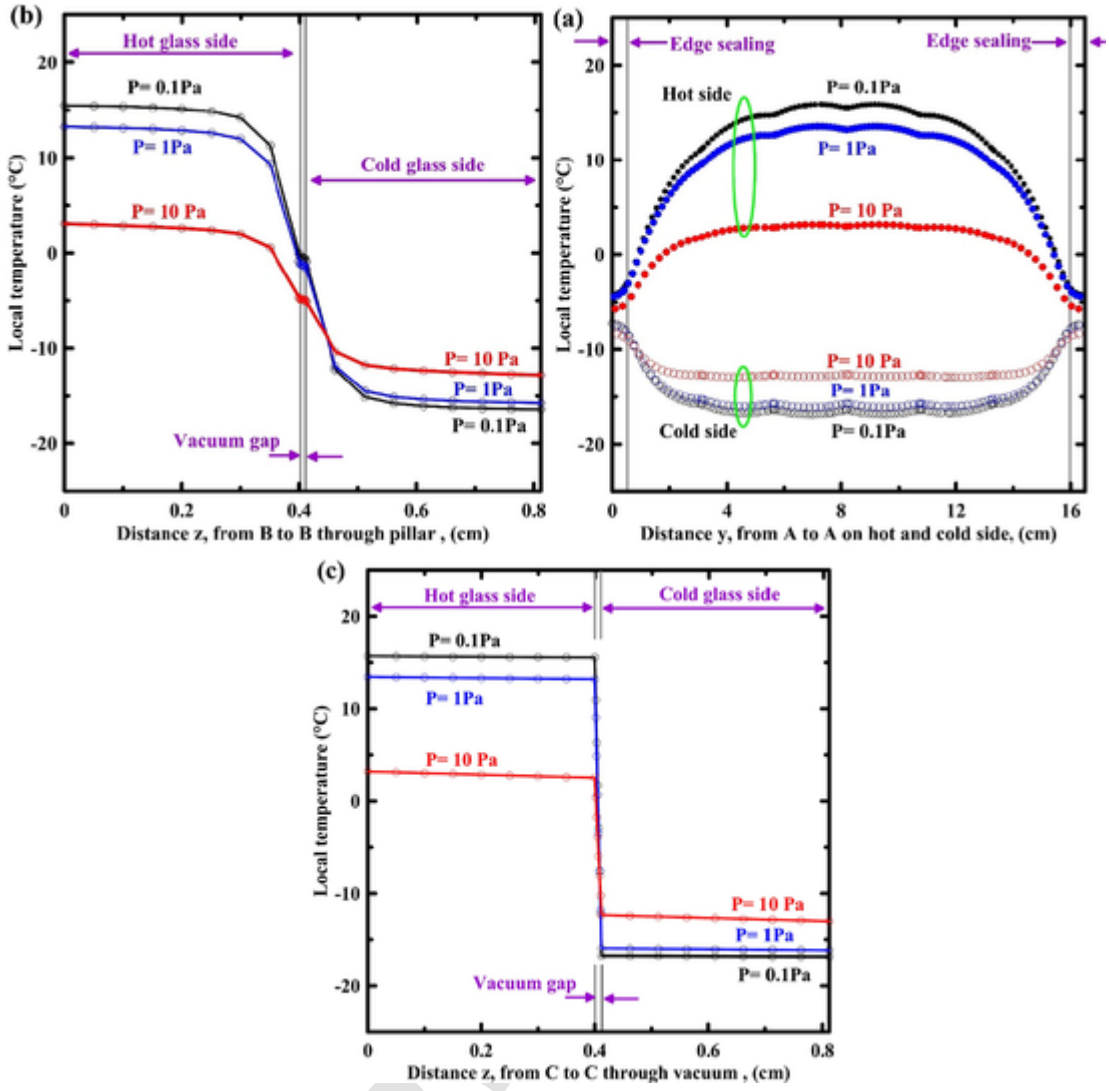

Fig. 11. Local temperature distribution at (a) lines (A-A) on the hot and cold sides of the VG window; (b) line (B-B) through pillar of the VG window and (c) line (C-C) through vacuum space of the VG window at different vacuum pressure levels.

ment is affected by the higher heat transfer coefficient closer to the cold side. Farther increase in the vacuum pressure to 10 Pa results in a higher cold side temperature of −11.9 °C.

Based on the VG results, it can be summarized that replacing the conventional double air-filled glazing with VG reduces the U-value from 6.37 $Wm^{-2}K^{-1}$ to approximately 3.1 $Wm^{-2}K^{-1}$, 3.3 $Wm^{-2}K^{-1}$, and 4.5 $Wm^{-2}K^{-1}$ at vacuum pressures of 0.1 Pa, 1 Pa, and 10 Pa respectively. However, these accomplished U-values are higher compared with the achieved U-values in the literature and in the markets. This is because the simulated VG has a dimensions of 15 cm × 15 cm that accounts the complete edge effects and not one-quarter of the VG was modelled but the whole VG. This means that the contribution of the edge sealing is dominant compared with the larger size VG in the markets. Therefore, using the VG in this small-scale applications decreases the U-value by only around 51.4%, 48.3%, and 29.4% at vacuum pressure of 0.1 Pa, 1 Pa, and 10 Pa respectively. This slight decrease in the U-value can be accomplished by using another new cost-effective option such as TVIP as a replacement to conventional glazed window.

3.1.2. Translucent vacuum insulation panel (TVIP)

The current section is used to show the previous trends for the new proposed TVIP with the same dimensions. In this section, TVIP, dimensions of 15 cm × 15 cm, is simulated. The effect of pressure deterioration on the thermal insulation performance are investigated. By the same method, the temperatures at different locations were displayed, then the temperature contours on the hot side also displayed. Fig. 15 shows the locations where the local temperatures are displayed. First, the lines A-A are located on the hot and cold side of the TVIP passing from one side to the other at the mid of the TVIP width. Other two lines B-B and C-C pass through the thickness of the TVIP the first through the vacuum region and the second through the frame material.

Fig. 16(a) show the temperature distribution over line A-A on the hot and cold side of the TVIP. A zoomed in region from the curve is depicted in Fig. 16(b). It is noticed that the hot side temperature increases with the increase in the vacuum pressure at the same location. In addition, the maximum temperature located at the center of the vacuum region. The lowest values of the temperatures locates at the frame section. This because of the higher thermal conductivity of the frame compared with the vacuum region. In more details, the temperature over the hot side temperature changes, from 1 °C to 15 °C, at the vacuum pressure of 0.1 Pa. Changing the vacuum pressure to 1 Pa and 10 Pa, A slight decrease in the hot side temperature in the frame section and significantly decreases the hot side temperature in the vacuum zone to around 12.5 °C and 5 °C respectively. However, the cold

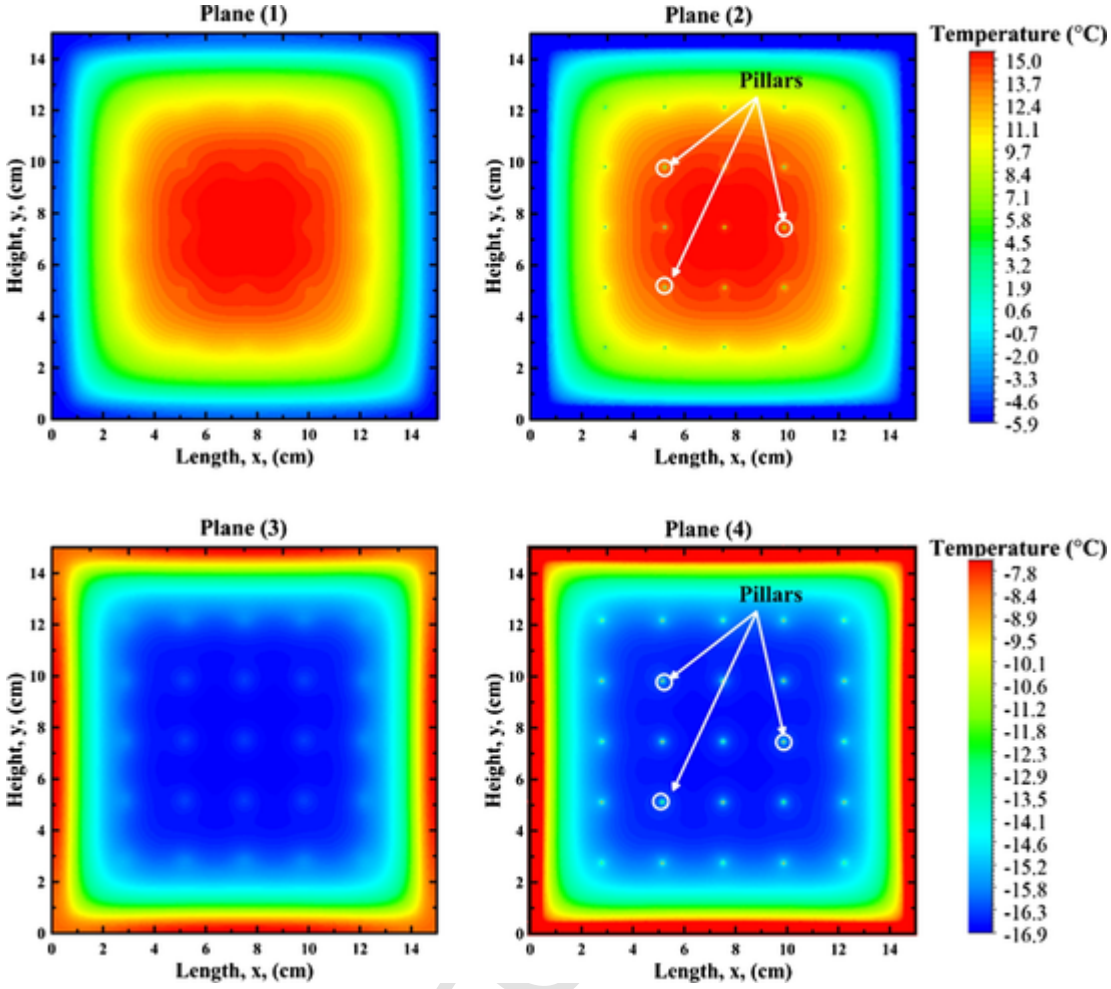

Fig. 12. Predicted temperature contours at vacuum pressure of 0.1 Pa at different planes or surfaces of the VG.

side temperature increases from −15.6 °C to −12.5 °C with increasing the vacuum pressure from 0.1 Pa to 10 Pa respectively. The temperature distribution over the cold side is constant with TVIP width. This is because the 3 mm glass layer located near to the cold side. One of the main interesting findings in such kind of comparison is no edge effects due to the absence of highly conductive edge-sealing material. However, the effect of thermal bridge through the frame structure is much pronounced compared with the VG. Therefore, more studies related to dimensions, thermal properties, and structure of the frame still needed to further overcome the thermal bridge effect through the spacer.

The temperature distributions through the TVIP window thickness through the vacuum region, line B-B, and through the frame region, line C-C, are shown in Fig. 16(c) and (d) respectively. As previously mentioned, the TVIP has a frame with total thickness of 3 mm attached to the conventional 3 mm glass. At line B-B in Fig. 16(c), the temperature significantly decreases from 16 °C to around −15.2 °C through the vacuum space whilst a very slight decrease of temperatures have been observed through the 3 mm glass layer. This is because of the significant reduction in the vacuum region thermal conductivity compared with the glass layer. It is also noticed that the temperature difference across the vacuum pane region decreases with the increase in the vacuum pressure. In more details, the temperature difference across the vacuum frame is about 31.2 °C, 25.5 °C, and 18 °C at vacuum pressure of 0.1 Pa, 1 Pa, and 10 Pa respectively.

On the other hand, the temperature at the location C-C are shown in Fig. 16(d). It shows the temperature were obtained through a 3 mm frame structure and then through the 3 mm glass layer. It is noticed that the temperature difference across the frame thickness were about 13.5 °C, 12.9 °C, and 10 °C at a vacuum pressures of 0.1 Pa, 1 Pa, and 10 Pa respectively. Also, a slight reduction across the glass pane is observed. However, the temperature difference across the glass pane in the frame region is slightly higher than that in the vacuum region. This is because of the lower heat transfer through the vacuum region compared with the heat transfer across the frame regions.

The temperature contours on the hot side of the TVIP at different vacuum pressures are shown in Fig. 17. Generally, at vacuum pressure of 0.1 Pa, the hot side temperature of the TVIP is very high and very closer to the indoor environment. In addition, the thermal bridge through the frame structure is also much pronounced. For instance, the temperature of the frame spacer on the hot side of the TVIP is about 1 °C under ASTM boundary conditions whilst the vacuum region temperatures are around 15 °C. This results in an area weighted average temperature of the hot side of the TVIP with about 12 °C at a vacuum pressure of 0.1 Pa. Further vacuum deterioration lead to a decrease of the hot side temperature to average values of 9.8 °C and 3.8 °C at vacuum pressure of 1 Pa and 10 Pa respectively.

It has been observed that the similar trends of temperatures obtained for the VG and TVIP. However, the main difference among them is that the VG has a smaller thermal bridge through the pillars compared with the frame spacer in the TVIP. Although, the TVIP has no edge effect like the VG has. Therefore, quantitative comparison between these two types of the glazing to the window insulation method is essential at various vacuum pressure and the window sizes.

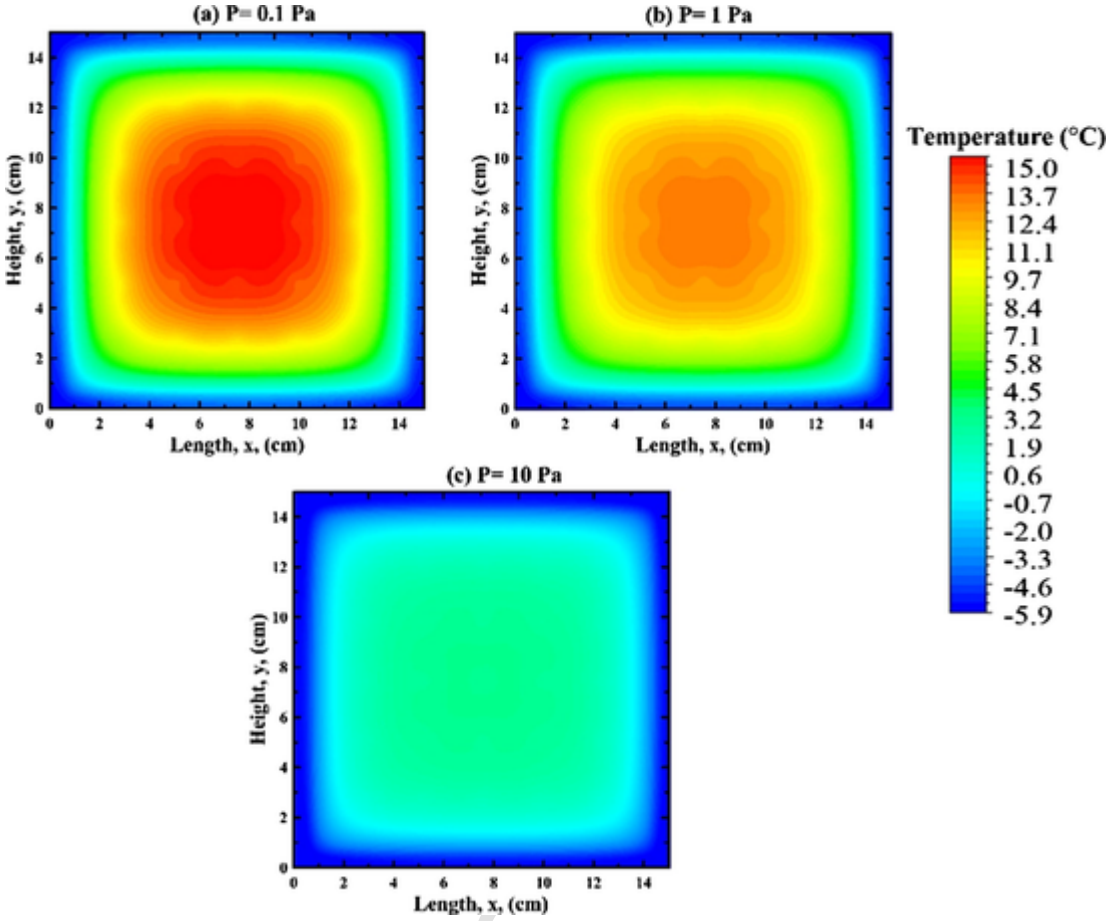

Fig. 13. Predicted temperature contours at the hot side, plane (1), of the VG at different vacuum pressure levels of (a) P = 0.1 Pa, (b) P = 1 Pa and (c) P = 10 Pa.

3.1.3. Comparison of VG and TVIP

This section quantitively compares the VG with TVIP under ASTM boundary conditions with dimensions of 15 cm × 15 cm at different vacuum pressures. In this comparison, the hot side and clod side area weighted average temperatures, average heat flux transfer, temperature differences across the glazing/panel sides, and the total glazing U-value are compared at different vacuum pressures of 0.1 Pa, 1 Pa, and 10 Pa in Fig. 18(a), (b), and (c) respectively.

Based on Fig. 18, the area weighted average hot side temperatures for the TVIP window is much higher compared with the same for the VG at the same pressure. In addition, the cold side temperature of the TVIP is much lower than the same for the VG at the same pressure. This mean that the mean temperature difference across the TVIP is higher than that for the VG. Therefore, better insulation performance can be obtained. This trend is observed over the entire investigated vacuum pressure range from 0.1 Pa to 10 Pa. This also confirms that using the TVIP is more favorable compared with VG even with vacuum deterioration problem occurs. Based on the U-value, it is noticed that the using the VG technology for small scale windows with 15 cm × 15 cm area accomplishes higher U-value of 3.1 $Wm^{-2}K^{-1}$ at vacuum pressure of 0.1 Pa because of the higher contribution of the edge effects. Whilst, using the TVIP achieved lower U-value of 1.9 $Wm^{-2}K^{-1}$ at the same vacuum pressure. Increasing the vacuum pressure, still the TVIP is favorable compared with the VG for smaller size of glazing. However, these results were influenced the size of the glazing specially for the VG. This is because increasing the glazing area, decreases the area ratio of the sealing region in the VG. Therefore, the edge sealing effect could be eliminated in a larger size VG and such comparison is essential.

3.2. Effect of glazing size on the thermal insulation performance of VG and TVIP

The ratio of the edge sealing area to the total glazing area decreases with the increase in the glazing size in VG. Using VG could be a promising thermal insulation method for the window with a larger area compared to the smaller area of the glazing. This is because of decreasing the edge effects. However, in TVIP, no edge effects and the thermal bridge through the frame structure is constant with changing the glazing size. This is because, increasing the glazing size does not affect the ratio between the frame zones and the vacuum region zones in the TVIP. Therefore, this section compares the performance of the VG and TVIP at different glazing sizes. The investigated glazing's have a square area with edge length changes from 15 cm up to 100 cm. The comparison is implemented based on the quantitative comparison of the predicted U-value and the maximum temperature difference across the glazing in Fig. 19(a) and Fig. 19(b) respectively. This comparison is conducted at different vacuum pressure levels.

In Fig. 19(a), the variation of U-value for the VG and TVIP with the glazing edge length at different vacuum pressure is shown. In this comparison a square glazing shape is simulated. Generally, it is obvious that increasing the glazing area or the glazing width decreases the U-value of the VG while the U-value remains constant for the TVIP. This is because increasing the glazing area decreases the edge sealing effect in VG. While the TVIP doesn't have edge sealing problem. In addition, increasing the vacuum pressure increases the U-value for all these sys-

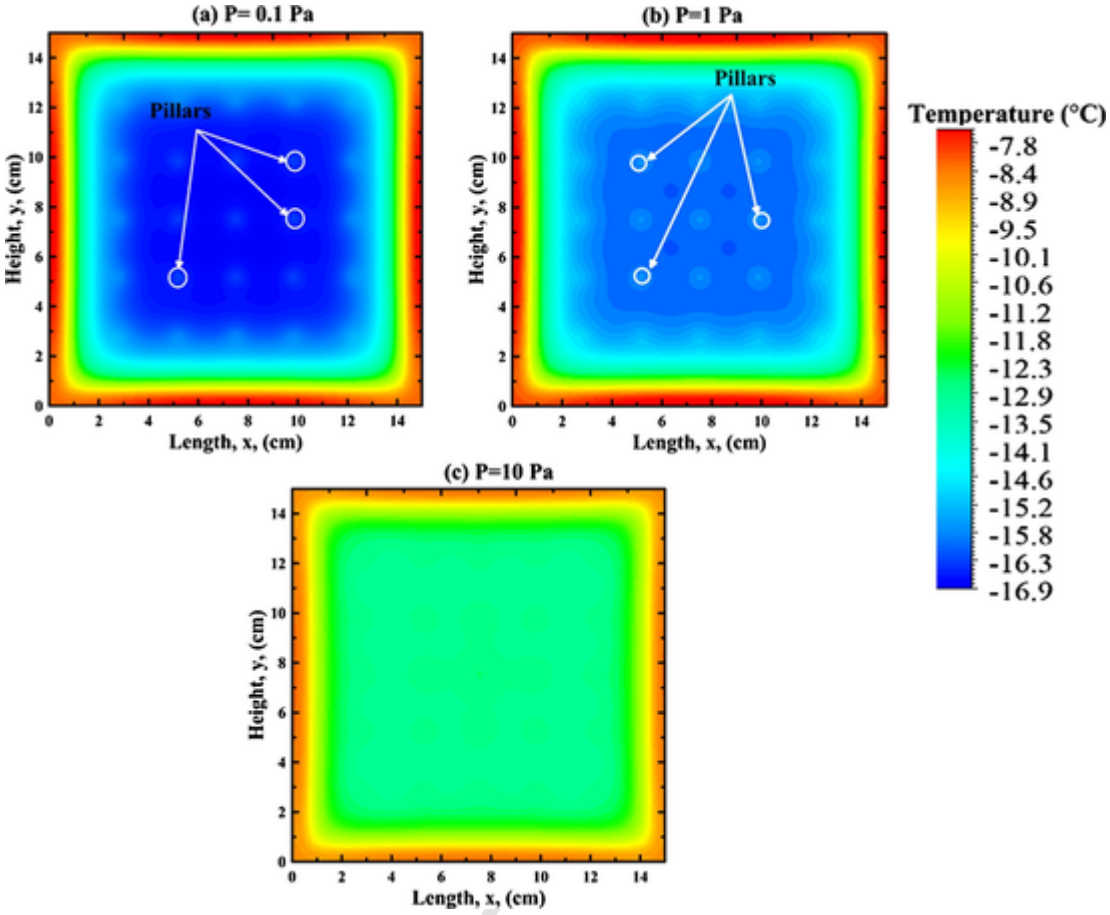

Fig. 14. Predicted temperature contours at the cold side, plane (3), of the VG at different vacuum pressure levels of (a) P = 0.1 Pa, (b) P = 1 Pa and (c) P = 10 Pa.

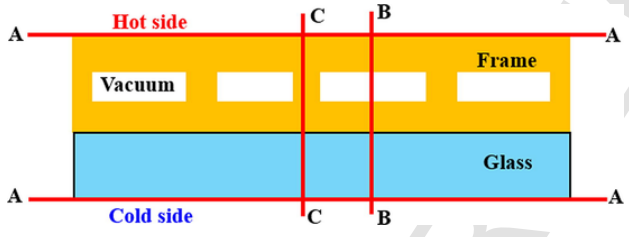

Fig. 15. Locations where the results were displayed.

tems over the all the glazing sizes. It is also worth mentioning that the applicability of both VG and TVIP is a function of glazing sizes. In more details, at a vacuum pressure of 0.1 Pa, the TVIP achieves lower U-value compared with the VG when the glazing area is less than 34 cm × 34 cm. However, increasing the glazing size above this area, the VG achieves lower U-value. Further, deteriorating the vacuum pressure to 1 Pa lead to increase the U-value for both TVIP and VG. At this condition, the TVIP as a glazing is favorable in terms of thermal insulation performance of glazing with area less than 30 cm × 30 cm. Increasing the glazing area above this value the VG achieves better thermal insulation performance. It has also been noticed that when TVIP compared with VG over the entire area of the glazing at higher vacuum pressure of 10 Pa, TVIP performs better than VG. This is because at lower vacuum pressures the thermal conductivity of the vacuum space increases whilst the thickness of the vacuum space in the VG is less than that in the TVIP. Therefore, the thermal resistance of the TVIP become higher than that for the VG at vacuum pressure of 10 Pa. In Fig. 19(b), the variation of maximum temperature difference across the glazing area is displayed with the edge length at different vacuum pressures for VG and TVIP. Three main conclusions can be summarized here. First, increasing the glazing area or the width of the edge-seal increases ΔT for the VG whilst it is nearly constant for the TVIP. Second, increasing the pressure decreases ΔT for both VG and TVIP at the same glazing area. And third, the TVIP achieves higher ΔT compared with VG at vacuum pressures of 10 Pa over the different sizes of glazing.

3.3. Comparison of different scenarios of the proposed designs

In this section, four different cases of the VG and TVIP with different structure were compared. Table 5 shows the details of each case. The simulation is conducted at a vacuum pressure of 0.1 Pa and square glazing's area of 15 cm × 15 cm as a sample of results.

Based on the investigated cases, it is noticed that at the same total thickness of the VG and TVIP samples, Case (3) and Case (1), still the TVIP accomplish lower U-value compared with the VG at the investigated glazing's area. In addition, comparing case (2) and case (3), increasing the vacuum thickness of the TVIP slightly decrease the U-value. In more details, increasing the vacuum thickness from 3 mm to 5 mm decrease the U-value by about 0.18 Wm^2K^{-1} at the same conditions.

Indium-edge seled VG is one of the low-temperature sealed method, case (4) propose the theoretical applicability of holding the VG components using gas barrier envelope instead of indium. Therefore, by comparing case (4) with case (1), it is evident that the use of gas barrier envelope in the VG is a favorable option to decreases the U-value. In more details, the U- value significantly decreased from 3.1 Wm^2K^{-1} to 0.65 Wm^2K^{-1}. This decrease is due to the elimination of the thermal bridge through the edge sealing. Therefore, the practicality of this

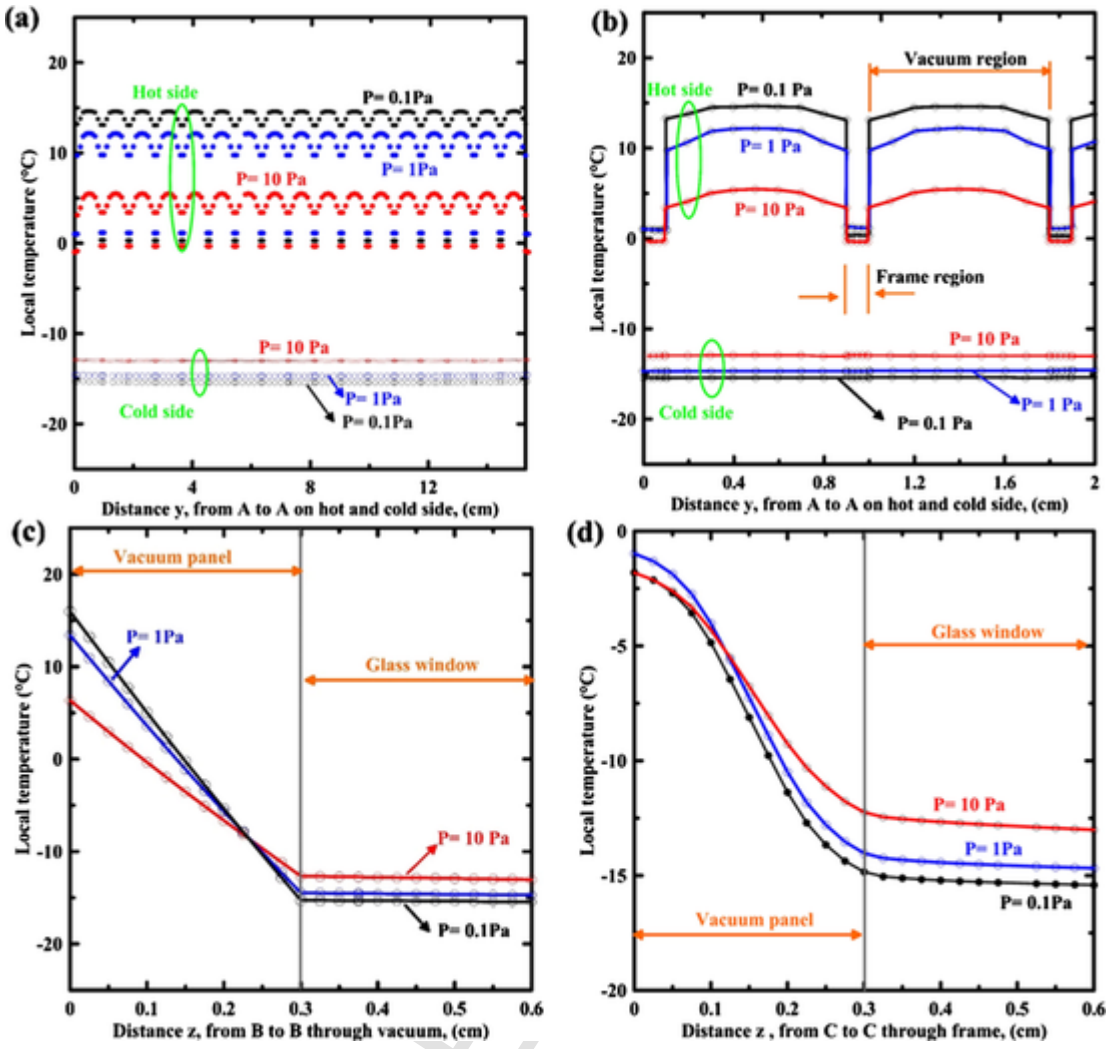

Fig. 16. Effect of changing the pressure deterioration on the predicted local temperatures at (a) lines (A-A) on the hot and cold sides of the TVIP with 3 mm glass layer; (b) zoomed in scale of local temperatures shown in (a); (c) line (B-B) through vacuum region of the TVIP; and (d) line (C-C) through frame of the TVIP.

case must be revisited to discover the fabrication and implementation issues that may face in the future work. Further, the temperature contours on the hot and the cold side of case (4) were depicted in Fig. 20. The thermal bridge through the edge sealing is completely eliminated. While the thermal bridge through the pillars became clearer.

3.4. Cost analysis comparison of VG and TVIP windows

Cost is a substantial challenge in determining if VG is cost-effective or affordable to consumers. The cost analysis presented here is the total cost in US dollars per m^2 of VG and TVIP and is based on the cost at the laboratory scale. This cost analysis does not include the electricity and time it take to construct VG and TVIP because it would be dependent on how the construction processes can be automated. It is also pertinent to mention here that the materials cost is dependent on the supplying company's location, quantity required, and purity of products supplied. A further important factor to consider is the wide variation in market prices of semi-precious metals such as indium alloy. This analysis is based only on the laboratory-based experiments and materials cost at the mass manufacturing level will be reduced significantly and will depend on the metal stock exchange rate. The laboratory scale costs of the materials used are presented in the Table 6. In this subsection, the cost of the VG and TVIP glazing are compared.

Table 6 shows that the cost of constructing VG is more than three times to the cost of TVIP. It shows that the edge sealing material, in this case used as Indium alloy, is a major contributing factor. This analysis is based only on the laboratory-based experiments and materials cost at the mass manufacturing level will be reduced significantly but the overall influence to the comparison of VG and TVIP could be similar.

4. Conclusions

In the present study, a new structured core translucent vacuum insulation panel (TVIP), as a retrofitting proposal to the conventional glazed windows to nearly zero energy buildings, in comparison to vacuum glazing (VG) technology is presented. In this TVIP, this total thickness of 3 mm frame with Low-emissive coated film were kept inside a transparent envelope and attached to 3 mm glass layer of glazing were used. The effect of vacuum pressure deterioration on the thermal insulation performance of VG and TVIP glazing's were compared at different glazing sizes. A three-dimensional finite-volume model is developed and validated with the experiments and data in the literature. In the recent investigations, only quarter of the VG was modelled. However, in the current model, the whole glazing area was modelled to capture the full effect of the edge sealing in VG. Based on the simulation results, the following conclusions are summarized:-

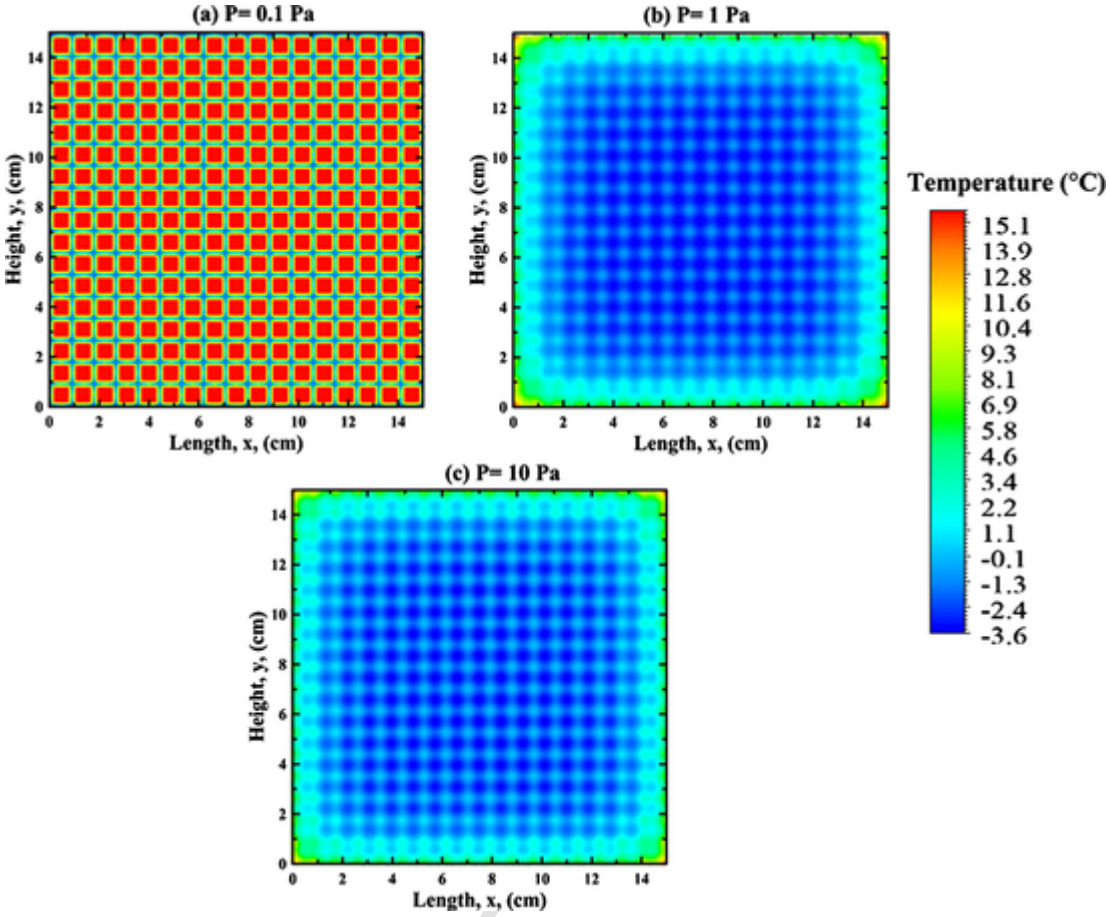

Fig. 17. Predicted temperature contours at the hot side of the TVIP at different vacuum pressure levels.

i. The proposed TVIP has no edge-effects when compared to VG.
ii. At vacuum pressure of 0.1 Pa, the TVIP achieved lower U-value compared with the VG when the glazing area is less than 34 cm × 34 cm. However, increasing the glazing size above this area, the VG achieves lower U-value.
iii. When the vacuum pressure is deteriorated to 1 Pa, an increase of the U-value for both TVIP and VG was predicted. At this condition, the TVIP is favorable option for thermal insulation to windows with area less than 30 cm × 30 cm. Increasing the glazing area above this value the VG achieves better insulation performance.
iv. The TVIP performance is compared with VG over the entire area of the glazing at higher vacuum pressure of 10 Pa and it was found that TVIP performed better.
v. The TVIP cost is about three times less than the cost of VG.
vi. Replacing the indium sealing in VG with gas barrier envelope theoretically eliminate the edge sealing effect. However, the practicality of this design must be revisited in a future work.

Declaration of Competing Interest

The authors declared that there is no conflict of interest.

Acknowledgement

This research work was supported by Daiwa Anglo-Japanese Foundation Grant (12549/13360) (Project Leader: Dr Saim Memon and Project Partner: Dr Takao Katsura). The authors are grateful of impeccable research collaboration between Hokkaido University, Japan, and London South Bank University, UK achieved with this grant.

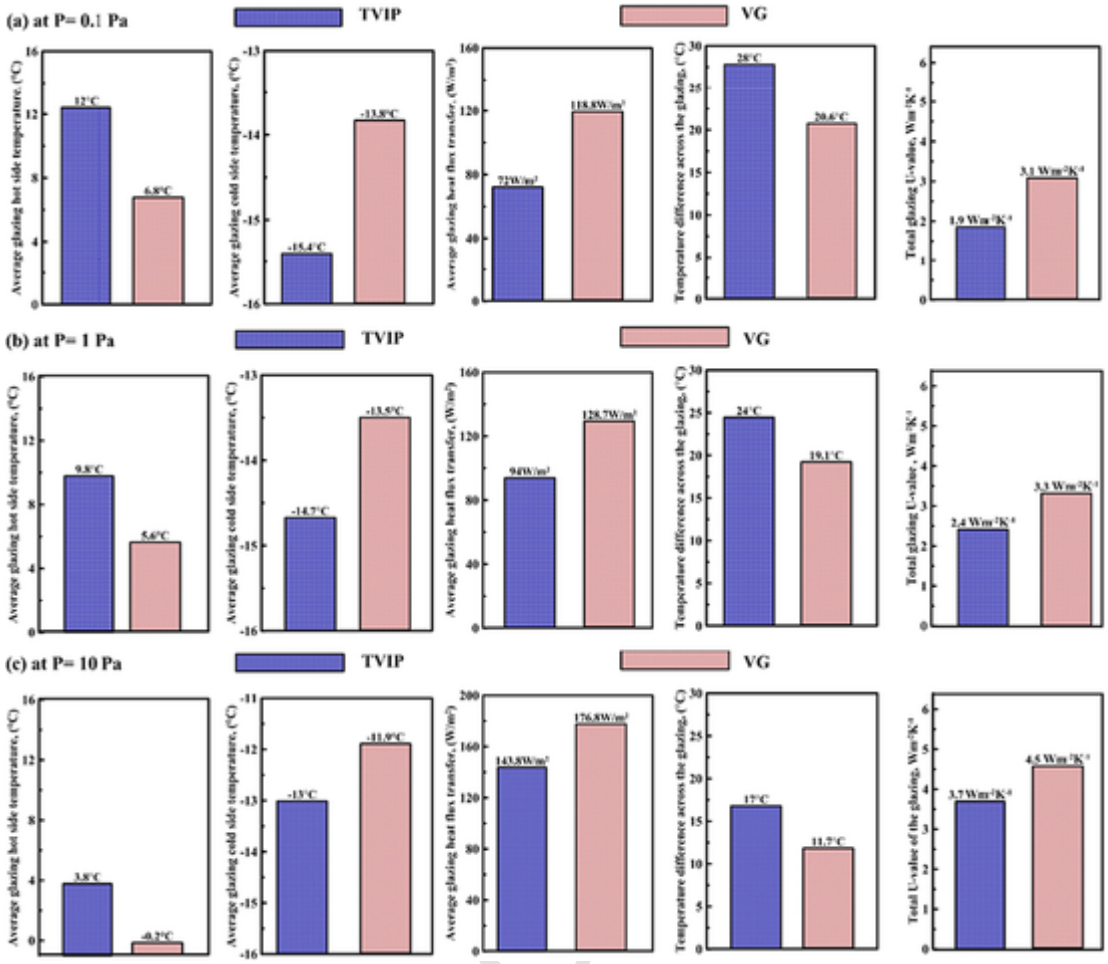

Fig. 18. Quantitative comparisons between the VG and VIP dimensions of 15 cm × 15 cm under ASTM boundary conditions at (a) P = 0.1 Pa; (b) P = 0.1 Pa ; and (c) P = 0.1 Pa.

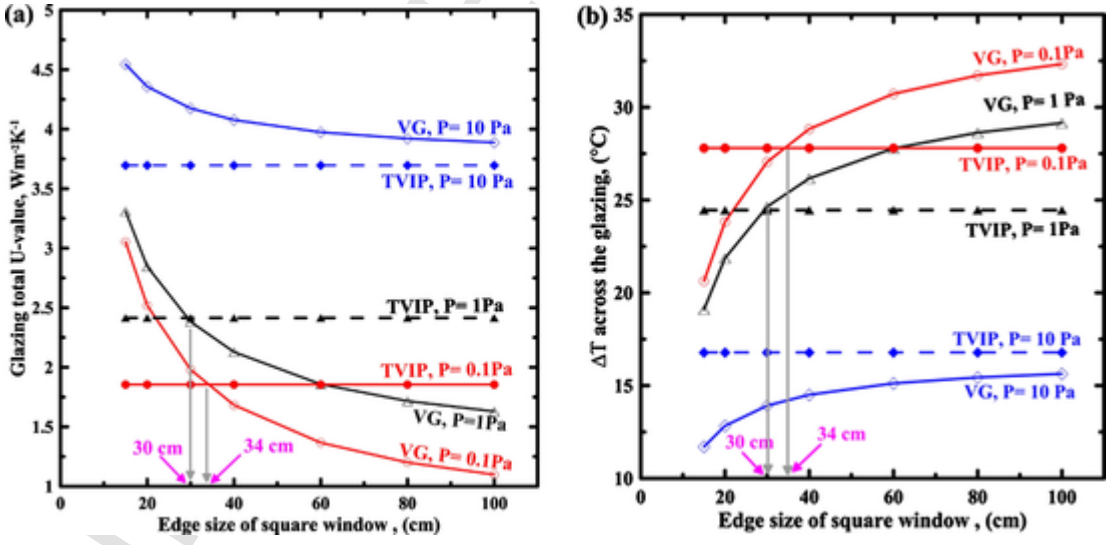

Fig. 19. Simulation results of (a) U-value for the VG and TVIP and (b) temperature difference, ΔT, across the glazing area at different dimensions.

Table 5
Different scenarios for different designs of the VG and TVIP.

Cases	Details	Predicted U-value
Case (1)	Commercial VG with 0.12 mm vacuum thickness, total sample thickness of 8.12 mm, indium sealed with 6 mm width. (Reference case of VG)	3.1 $Wm^{2}K^{-1}$
Case (2)	Conventional TVIP with 3 mm vacuum thickness, and 3 mm glazing. (Reference case of TVIP)	1.9 $Wm^{2}K^{-1}$
Case (3)	TVIP with total thickness equal to the total thickness of the VG as in Case (1). The sample has a 3 mm glass layer and the vacuum thickness increased to 5.12 mm.	1.72 $Wm^{2}K^{-1}$
Case (4)	VG sample as in Case (1) except the gas barrier envelope is used to hold the VG components without indium sealing.	0.65 $Wm^{2}K^{-1}$

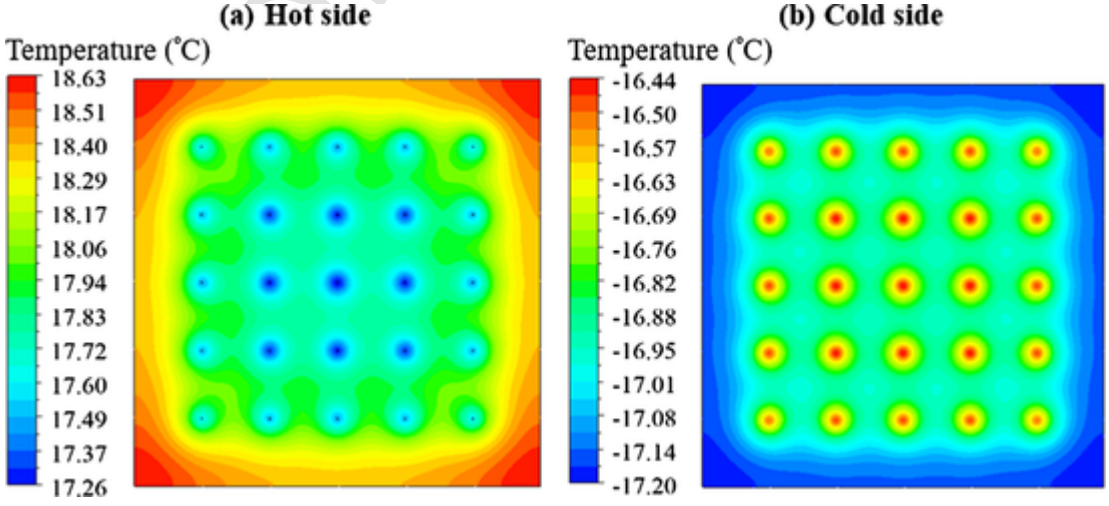

Fig. 20. Temperature contours on the hot and cold sides of the VG sample with gas barrier envelope instead of indium sealing as in Case (4).

Table 6
Material cost used in the construction process of the VG and TVIP windows ($/m^2).

Glazing type	Components	Cost ($/m^2)
VG	Low-e coated glass pane	8
	Pillars	30
	Edge-sealing material	250
	Construction cost	50
	Total material cost	338
TVIP	3 mm glass pane	8
	Frame structure	18
	Envelope	18
	L-e coating film	45
	Adsorbent material	6
	Construction cost	12
	Total material cost	107

References

Alam, M., Singh, H., Brunner, S., Naziris, C., 2014. Experimental characterisation and evaluation of the thermo-physical properties of expanded perlite—Fumed silica composite for effective vacuum insulation panel (VIP) core. Energy Build. 69, 442–450. doi:10.1016/j.enbuild.2013.11.027.

ANSYS FLUENT Theory Guide, 2011.

Arya, F., Moss, R., Hyde, T., Shire, S., Henshall, P., Eames, P., 2018. Vacuum enclosures for solar thermal panels part 1: fabrication and hot-box testing. Sol. Energy 174, 1212–1223. doi:10.1016/j.solener.2018.10.064.

Baetens, R., Jelle, B.P., Thue, J.V., Tenpierik, M.J., Grynning, S., Uvsløkk, S., Gustavsen, A., 2010. Vacuum insulation panels for building applications: a review and beyond. Energy Build. 42, 147–172. doi:10.1016/j.enbuild.2009.09.005.

Brambilla, A., Salvalai, G., Imperadori, M., Sesana, M.M., 2018. Nearly zero energy building renovation: From energy efficiency to environmental efficiency, a pilot case study. Energy Build. 166, 271–283. doi:10.1016/j.enbuild.2018.02.002.

Choi, B., Yeo, I., Lee, J., Kang, W.K., Song, T.H., 2016. Pillar-supported vacuum insulation panel with multi-layered filler material. Int. J. Heat Mass Transf. 102, 902–910. doi:10.1016/j.ijheatmasstransfer.2016.06.032.

Chuntonov, K., Ivanov, A.O., Verbitsky, B., Setina, J., 2018. Getters for vacuum insulated glazing. Vacuum 155, 300–306. doi:10.1016/j.vacuum.2018.06.012.

Di, X., Gao, Y., Bao, C., Hu, Y., Xie, Z., 2013. Optimization of glass fiber based core materials for vacuum insulation panels with laminated aluminum foils as envelopes. Vacuum 97, 55–59. doi:10.1016/j.vacuum.2013.04.005.

Eames, P.C., 2008. Vacuum glazing: current performance and future prospects. Vacuum 82, 717–722. doi:10.1016/j.vacuum.2007.10.017.

Fang, Y., Arya, F., 2019. Evacuated glazing with tempered glass. Sol. Energy 183, 240–247. doi:10.1016/j.solener.2019.03.021.

Fang, Y., Hyde, T., Eames, P.C., Hewitt, N., 2009. Theoretical and experimental analysis of the vacuum pressure in a vacuum glazing after extreme thermal cycling. Sol. Energy 83, 1723–1730. doi:10.1016/j.solener.2009.03.017.

Fang, Y., Hyde, T., Hewitt, N., Eames, P.C., Norton, B., 2009. Comparison of vacuum glazing thermal performance predicted using two- and three-dimensional models and their experimental validation. Sol. Energy Mater. Sol. Cells 93, 1492–1498. doi:10.1016/j.solmat.2009.03.025.

Fang, Y., Hyde, T.J., Arya, F., Hewitt, N., Eames, P.C., Norton, B., Miller, S., 2014. Indium alloy-sealed vacuum glazing development and context. Renew. Sustain. Energy Rev. 37, 480–501. doi:10.1016/j.rser.2014.05.029.

Fang, Y., Memon, S., Peng, J., Tyrer, M., Ming, T., 2020. Solar thermal performance of two innovative configurations of air-vacuum layered triple glazed windows. Renew. Energy 150, 167–175. doi:10.1016/j.renene.2019.12.115.

Fischer-Cripps, A.C., Collins, R.E., Turner, G.M., Bezzel, E., 1995. Stresses and fracture probability in evacuated glazing. Build. Environ. 30, 41–59. doi:10.1016/0360-1323(94)E0032-M.

Ghosh, A., Norton, B., 2018. Advances in switchable and highly insulating autonomous (self-powered) glazing systems for adaptive low energy buildings. Renew. Energy 126, 1003–1031. doi:10.1016/j.renene.2018.04.038.

Ghosh, A., Norton, B., Duffy, A., 2016. Measured thermal & daylight performance of an evacuated glazing using an outdoor test cell. Appl. Energy 177, 196–203. doi:10.1016/j.apenergy.2016.05.118.

Griffiths, P.W., Eames, P.C., Hyde, T.J., Fang, Y., Norton, B., 2006. Experimental characterization and detailed performance prediction of a vacuum glazing system fabricated with a low temperature metal edge seal, using a validated computer model. J. Sol. Energy Eng. Trans. ASME 128, 199–203. doi:10.1115/1.2188529.

Huang, H., Zhou, Y., Huang, R., Wu, H., Sun, Y., Huang, G., Xu, T., 2020. Optimum insulation thicknesses and energy conservation of building thermal insulation materials in Chinese zone of humid subtropical climate. Sustain. Cities Soc. 52, 101840. doi:10.1016/j.scs.2019.101840.

Johansson, P., Hagentoft, C.E., Sasic Kalagasidis, A., 2014. Retrofitting of a listed brick and wood building using vacuum insulation panels on the exterior of the facade: measurements and simulations. Energy Build. 73, 92–104. doi:10.1016/j.enbuild.2014.01.019.

Jung, H., Yeo, I., Song, T.H., 2014. Al-foil-bonded enveloping and double enveloping for application to vacuum insulation panels. Energy Build. 84, 595–606. doi:10.1016/j.enbuild.2014.08.045.

Kalnæs, S.E., Jelle, B.P., 2014. Vacuum insulation panel products: a state-of-the-art review and future research pathways. Appl. Energy 116, 355–375. doi:10.1016/j.apenergy.2013.11.032.

Katsura, T., Radwan, A., Yang, Z., Nakamura, M., Nagano, K., 2019. Energy conservation using new structured-core and transparent vacuum insulation panels: Numerical simulation with experimental validation. Sol. Energy 193, 885–905. doi:10.1016/j.solener.2019.09.083.

Kim, J., Lee, J.H., Song, T.H., 2012. Vacuum insulation properties of phenolic foam. Int. J. Heat Mass Transf. 55, 5343–5349. doi:10.1016/j.ijheatmasstransfer.2012.05.051.

Kim, J., Song, T.H., 2013. Vacuum insulation properties of glass wool and opacified fumed silica under variable pressing load and vacuum level. Int. J. Heat Mass Transf. 64, 783–791. doi:10.1016/j.ijheatmasstransfer.2013.05.012.

Kisilewicz, T., Fedorczak-Cisak, M., Barkanyi, T., 2019. Active thermal insulation as an element limiting heat loss through external walls. Energy Build. 205, 109541. doi:10.1016/j.enbuild.2019.109541.

Kwon, J.S., Jang, C.H., Jung, H., Song, T.H., 2009. Effective thermal conductivity of various filling materials for vacuum insulation panels. Int. J. Heat Mass Transf. 52, 5525–5532. doi:10.1016/j.ijheatmasstransfer.2009.06.029.

Kwon, J.S., Jung, H., Yeo, I.S., Song, T.H., 2011. Outgassing characteristics of a polycarbonate core material for vacuum insulation panels. Vacuum 85, 839–846. doi:10.1016/j.vacuum.2010.12.009.

Memon, S., 2017. Experimental measurement of hermetic edge seal's thermal conductivity for the thermal transmittance prediction of triple vacuum glazing. Case Stud. Therm. Eng. 10, 169–178. doi:10.1016/j.csite.2017.06.002.

Memon, S., Eames, P.C., 2017. Predicting the solar energy and space-heating energy performance for solid-wall detached house retrofitted with the composite edge-sealed triple vacuum glazing. Energy Procedia 122, 565–570. doi:10.1016/j.egypro.2017.07.419.

Memon, S., Fang, Y., Eames, P.C., 2019. The influence of low-temperature surface induction on evacuation, pump-out hole sealing and thermal performance of composite edge-sealed vacuum insulated glazing. Renew. Energy 135, 450–464. doi:10.1016/j.renene.2018.12.025.

Memon, S., Farukh, F., Eames, P.C., Silberschmidt, V.V., 2015. A new low-temperature hermetic composite edge seal for the fabrication of triple vacuum glazing. Vacuum 120, 73–82. doi:10.1016/j.vacuum.2015.06.024.

Mukhopadhyaya, P., Kumaran, M.K., Normandin, N., Reenen, D. van, 2009. Fibre-powder composite as core material for vacuum insulation panel. 9th Int. Vac. Insul. Symp. 17th 18th Sept. 2009 R. Inst. Gt. Britain London.

Pérez-Lombard, L., Ortiz, J., Pout, C., 2008. A review on buildings energy consumption information. Energy Build. 40, 394–398. doi:10.1016/j.enbuild.2007.03.007.

Son, H., Song, T.H., 2019. Heat transfer and stress distribution in the central part of vacuum glazing. Appl. Therm. Eng. 159, 113926. doi:10.1016/j.applthermaleng.2019.113926.

Wang, Y., Chen, Z., Gu, Z., Sun, H., Yu, S., Nie, L., Luo, R., 2015. Preparation and thermal performance analysis of novel multilayer cladding structure composites. Mater. Des. 86, 633–639. doi:10.1016/j.matdes.2015.07.148.

Wilson, C.F., Simko, T.M., Collins, R.E., 1998. Heat conduction through the support pillars in vacuum glazing. Sol. Energy 63, 393–406. doi:10.1016/S0038-092X(98)00079-6.

Yang, Z., Katsura, T., Aihara, M., Nakamura, M., Nagano, K., 2018. Investigation into window insulation retrofitting of existing buildings using thin and translucent frame-structure vacuum insulation panels. Energies 11. doi:10.3390/en11020298.

Yang, Z., Katsura, T., Aihara, M., Nakamura, M., Nagano, K., 2017. Development of numerical heat transfer and the structural model to design slim and translucent vacuum layer type insulation panels to retrofitting insulation in existing buildings. Energies 10. doi:10.3390/en10122108.

Zhao, J.F., Eames, P.C., Hyde, T.J., Fang, Y., Wang, J., 2007. A modified pump-out technique used for fabrication of low temperature metal sealed vacuum glazing. Sol. Energy 81, 1072–1077. doi:10.1016/j.solener.2007.03.006.

Zhu, Q., Wu, W., Yang, Y., Han, Z., Bao, Y., 2020. Finite element analysis of heat transfer performance of vacuum glazing with low-emittance coatings by using ANSYS. Energy Build. 206, 109584. doi:10.1016/j.enbuild.2019.109584.